The meiotic LINC complex component KASH5 is an activating adaptor for cytoplasmic dynein

Kirsten E. L. Garner[1]*, Anna Salter[1,2]*, Clinton K. Lau[3], Manickam Gurusaran[4], Cécile Villemant[1], Elizabeth P. Granger[1], Gavin McNee[1], Philip G. Woodman[1], Owen R. Davies[4], Brian E. Burke[2]*, and Victoria J. Allan[1,2]*

*: equal contributions

1: School of Biological Sciences, Faculty of Biology, Medicine and Health, University of Manchester, The Michael Smith Building, Rumford St, Manchester M13 9PT.
2: A*STAR Institute of Medical Biology, 8A Biomedical Grove, #06-06 Immunos, Singapore 138648.
3: MRC Laboratory of Molecular Biology, Francis Crick Avenue, Cambridge Biomedical Campus, Cambridge CB2 0QH, UK
4: Wellcome Centre for Cell Biology, Institute of Cell Biology, University of Edinburgh, Michael Swann Building, Max Born Crescent, Edinburgh EH9 3BF, UK

Present addresses: Brian Burke, A*STAR Skin Research Labs (A*SRL), Biopolis, 8A Biomedical Grove, #06-06 Immunos, Singapore; Elizabeth Granger, University of Central Lancashire, Preston, PR1 2HE, UK; Gavin McNee, University of Birmingham, Edgbaston, Birmingham B15 2TT; Anna Salter, Immunocore Ltd, 92 Park Drive, Milton Park, OX14 4RY, UK; Cécile Villemant, The Automation Partnership, (Cambridge) Limited, York Way, Royston, Hertfordshire, SG8 5WY, UK

Corresponding author: Viki Allan (viki.allan@manchester.ac.uk), ORCID 0000-0003-4583-0836

Abstract

Cytoplasmic dynein-driven movement of chromosomes during prophase I of meiosis is essential for synapsis and genetic exchange. Dynein connects to chromosome telomeres via KASH5 and SUN1/2, which span the outer and inner nuclear envelopes, respectively. Here, we show that KASH5 promotes dynein motility in vitro, and cytosolic KASH5 inhibits dynein's interphase functions. KASH5 interacts with either dynein light intermediate chain (DYNC1LI1 or DYNC1LI2) via a conserved linker-helix in the LIC C-terminal, and this region is also needed for dynein's recruitment to other cellular membranes. KASH5's N-terminal EF-hands are essential, as the interaction with dynein is disrupted by mutation of key calcium-binding residues, although it is not regulated by cellular calcium levels. Dynein can be recruited to KASH5 at the nuclear envelope independently of dynactin, while LIS1 is essential for dynactin incorporation into the KASH5-dynein complex. Altogether, we show that the trans-membrane protein KASH5 is an activating adaptor for dynein, and shed light on the hierarchy of assembly of KASH5-dynein-dynactin complexes.

Introduction

To conceive healthy offspring, a paternal sperm and maternal egg must be created, which requires the specialised form of cell division, meiosis. During the long meiotic prophase I, sister chromatids attach to the nuclear envelope via their telomeres, and move along the inner nuclear membrane (INM) to transiently cluster in a 'meiotic bouquet' (Fig. S1 A) which enables the formation of the synaptonemal complex in zygotene (Chikashige et al., 2006; Koszul et al., 2008; Trelles-Sticken et al., 2005). This facilitates synapsis and recombination between homologous chromosomes, which is essential for meiotic progression and the generation of two genetically distinct haploid daughter cells (Hamer et al., 2008; Liu et al., 2019; Zhang et al., 2019). These dynamic chromosome movements require force generated by the microtubule motor cytoplasmic dynein-1 (Burke, 2018; Horn et al., 2013; Lee et al., 2015; Lee and Burke, 2018; Morimoto et al., 2012; Rog and Dernburg, 2015; Sato et al., 2009; Wynne et al., 2012). Crucially, the force must be transmitted from the cytoplasm to the chromosomes on the other side of the nuclear envelope. This is achieved by Linkers of Nucleoplasm and Cytoplasm (LINC complexes) which span the nuclear envelope to physically connect the cytoskeleton and nucleus (Burke, 2018; Lee and Burke, 2018; Sato et al., 2009; Spindler et al., 2019) (Fig. S1 A).

LINC complexes consist of SUN (Sad1, Unc-84) domain proteins that span the INM, binding nuclear lamins and chromatin associated proteins in the nucleoplasm, and interacting with KASH (**K**larsicht, **A**NC-1, **S**yne **H**omology) domain proteins. KASH proteins have large cytosolic domains that bind cytoskeleton-associated proteins and are anchored in the ONM by a C-terminal transmembrane domain (Bone and Starr, 2016; Burke, 2018). Inside the nuclear envelope lumen, the 50-60 amino acid C terminal KASH-domain sequence associates with SUN proteins, restricting the KASH protein localisation to the nuclear membrane (Morimoto et al., 2012; Starr, 2011; Starr and Han, 2002). The meiotic LINC complex contains SUN1 and SUN2, which have largely redundant roles (Ding et al., 2007; Link et al., 2014; Schmitt et al., 2007). They bind to a meiotic telomere complex (Dunce et al., 2018; Shibuya et al., 2014), and to KASH5 in vertebrates, which recruits dynein in the cytoplasm to transmit the mechanical force required for synapsis to telomeres (Horn et al., 2013; Morimoto et al., 2012) (Fig. S1 A). The critical importance of KASH5 during meiosis is exemplified by the *KASH5*$^{-/-}$ *null* mouse, which is completely sterile due to impaired synapsis

and resulting meiotic arrest (Horn et al., 2013). Human mutations in the transmembrane domain that cause mistargeting of KASH5 to mitochondria lead to male sterility (Bentebbal et al., 2021). KASH5 shares sequence homology with the N-terminal region of the protein encoded by the zebrafish gene *futile cycle* which is required for pronuclear migration (Dekens et al., 2003; Lindeman and Pelegri, 2012), another dynein-dependent function in which the female pronucleus uses dynein to migrate towards the male pronucleus along microtubules nucleated from the male centrosome (Gönczy et al., 1999; Payne et al., 2003; Reinsch and Karsenti, 1997; Robinson et al., 1999). The KASH protein responsible for pronuclear migration in mammals is not yet known.

Cytoplasmic dynein-1 (dynein, hereafter) transports a diverse range of cargo to the minus end of microtubules (Reck-Peterson et al., 2018). It is a large 1.6 MDa holoenzyme comprised of two heavy chains (DHC: DYNC1H1) containing the globular motor domains, which are the site of ATP hydrolysis. Its cargo binding tail domain contains the intermediate chains (ICs: DYNC1I1 and 2) which bind directly to the DHCs; three light chains (LCs), which bind to the ICs; and two light intermediate chains (LICs: DYNC1LI1 and 2) (Pfister et al., 2005; Reck-Peterson et al., 2018). The LICs bind to DHC via their N terminal GTPase-like domain, although they are not thought to exhibit GTPase activity (Schroeder et al., 2014). The LICs have an unstructured carboxy terminus which protrudes from the motor complex (Celestino et al., 2019; Lee et al., 2018; Schroeder et al., 2014). While the GTPase-like domain sequence is highly conserved between LIC1 and 2, there is less homology in the C terminus apart from two regions of predicted alpha-helix (Celestino et al., 2019; Kumari et al., 2021b; Lee et al., 2020; Lee et al., 2018). As described below, this C-terminal domain mediates the interaction between dynein and the recently identified activating cargo adaptors.

Dynein requires the multi-component dynactin complex for function (Feng et al., 2020; Gill et al., 1991; King et al., 2003; McKenney et al., 2014; Schlager et al., 2014a; Schroer and Sheetz, 1991), although dynein and dynactin alone interact weakly (Baumbach et al., 2017; Chowdhury et al., 2015; Jha et al., 2017; Splinter et al., 2012; Urnavicius et al., 2015). A third component is needed for optimum motility and force generation *in vitro,* the 'activating adaptors' (Belyy et al., 2016; McKenney et al., 2014; Schlager et al., 2014a), and many have

been identified (for reviews see (Canty and Yildiz, 2020; Olenick and Holzbaur, 2019; Reck-Peterson et al., 2018)), which promote dynein function in several ways. Firstly, they strengthen the interaction between dynein and dynactin (Schroeder and Vale, 2016; Splinter et al., 2012) by forming extensive interactions with both components to generate a tripartite dynein-dynactin-adaptor (DDA) complex, or complexes with two dyneins per dynactin and adaptor (D_2DA) (Chowdhury et al., 2015; Grotjahn et al., 2018; Lau et al., 2021; Lee et al., 2020; Urnavicius et al., 2018; Urnavicius et al., 2015). Secondly, they release the dynein motor domains from the autoinhibited Phi conformation (Torisawa et al., 2014; Zhang et al., 2017), helping to align them for microtubule interaction (Chowdhury et al., 2015; Zhang et al., 2017). Finally, they recruit dynein and dynactin to cargo (for example (Horgan et al., 2010b; Schroeder and Vale, 2016; Splinter et al., 2012; Wang et al., 2019)).

The assembly and function of dynein adaptor complexes is promoted by the dynein regulator Lissencephaly-1 (LIS1). LIS1 is needed for many dynein functions (reviewed in (Markus et al., 2020) and is mutated in the neurodevelopmental disorder, Type-1 lissencephaly (Reiner et al., 1993), which results from defective neural migration and progenitor proliferation (Hirotsune et al., 1998; Markus et al., 2020). LIS1 enhances the formation of DDA complexes (Baumbach et al., 2017; Dix et al., 2013) and increases the frequency, velocity and duration of dynein complex movement (Baumbach et al., 2017; Dix et al., 2013; Fenton et al., 2021; Gutierrez et al., 2017). Recent mechanistic studies have shown that LIS1 binding to the dynein motor domain promotes the opening of the Phi complex ((Elshenawy et al., 2020; Gillies et al., 2022; Htet et al., 2020; Marzo et al., 2020; Qiu et al., 2019) reviewed in (Canty and Yildiz, 2020; Markus et al., 2020; Olenick and Holzbaur, 2019)), a conformation that may assemble more readily with adaptors as well as being more active. This may be how LIS1 increases the proportion of D_2DA complexes containing two dyneins (Elshenawy et al., 2020; Htet et al., 2020) which generate more force, move faster and are more processive than single dynein DDA complexes (Elshenawy et al., 2019; Sladewski et al., 2018; Urnavicius et al., 2018). Furthermore, LIS1 also contributes to the recruitment of dynein, dynactin and/or adaptors to cellular cargoes ranging from ribonucleoprotein particles (RNPs) (Dix et al., 2013), to membranes (Lam et al., 2010), Rab6-positive vesicles (Splinter et al., 2012), the nuclear envelope (Cockell et al.,

2004; Sitaram et al., 2012; Splinter et al., 2012), spindle poles (Sitaram et al., 2012; Wang et al., 2013) and kinetochores (Dzhindzhev et al., 2005; Siller et al., 2005).

Activating adaptor proteins share little sequence homology, but generally contain a long coiled coil domain, and a site for cargo binding (Lee et al., 2020; McKenney et al., 2014; Redwine et al., 2017; Schlager et al., 2014a; Schlager et al., 2014b; Urnavicius et al., 2015). They all interact with the C-terminal domain of LICs via at least three distinct types of sequence motif: the CC1 box; the Hook domain; or EF hands (Celestino et al., 2019; Gama et al., 2017; Lee et al., 2020; Lee et al., 2018; Schroeder and Vale, 2016), and the motility of all three types of DDA complex is promoted by LIS1 (Htet et al., 2020). Other adaptors may not activate dynein, but still serve to link the motor to cargoes (Olenick and Holzbaur, 2019; Reck-Peterson et al., 2018). An example is Rab7-interacting lysosomal protein (RILP), which recruits dynein and dynactin to Rab7 positive late endosomes/lysosomes (Johansson et al., 2007; Jordens et al., 2001; Scherer et al., 2014; Tan et al., 2011) via its RILP homology domains, but lacks a long coiled coil. KASH5 is a good candidate to be an activating adaptor, because it contains an N-terminal EF-hand domain that binds dynein, followed by a long coiled coil (Horn et al., 2013; Morimoto et al., 2012). However, unlike other activating adaptors characterised so far, it is a trans-membrane protein.

Mammalian dynein contains either two LIC1 subunits, or two LIC2 subunits (Tynan et al., 2000a), thus providing the potential for differential interactions with adaptors. However, both LICs bind to the adaptors Rab11-FIP3 (Celestino et al., 2019; Horgan et al., 2010a; Horgan et al., 2010b), RILP (Celestino et al., 2019; Scherer et al., 2014), BICD2, spindly, Hook3, ninein and TRAK1 (Celestino et al., 2019), via the highly conserved helix 1 in the LIC C-terminus. This shared binding ability suggests that LICs may act redundantly, as has been reported in the endocytic pathway (Horgan et al., 2010a; Horgan et al., 2010b; Tan et al., 2011). However, other endocytic functions may be isoform-specific (Bielli et al., 2001; Hunt et al., 2013; Palmer et al., 2009). Likewise, although LIC1 and 2 act redundantly for some mitotic functions (Jones et al., 2014; Raaijmakers et al., 2013), isoform-specific functions and localisations have been reported during mitosis (Horgan et al., 2011; Mahale et al., 2016a; Mahale et al., 2016b; Palmer et al., 2009; Raaijmakers et al., 2013; Sharma et al., 2020; Sivaram et al., 2009), at the centrosome (Tynan et al., 2000b), during neuronal

nuclear migration (Goncalves et al., 2019) and cell migration (Even et al., 2019; Schmoranzer et al., 2009). In addition, mitotic phosphorylation of the LIC1 C-terminal domain may provide temporal control of adaptor selection (Kumari et al., 2021a). The degree of specific and shared functions for LICs is an important issue that is not fully resolved.

How the dynein motor interacts with KASH5 to drive the dynamic chromosome movements essential for meiosis has remained unknown. Here, we reveal the transmembrane protein KASH5 to be a novel member of the dynein activating adaptor class that interacts with the LIC helix 1 region. We demonstrate that this region in the LIC is also key for dynein's function at the Golgi apparatus and throughout the endocytic pathway, with LICs 1 and 2 acting redundantly in these locations. Analysis of the hierarchy of adaptor complex assembly reveals that dynein can be recruited to KASH5 independently of dynactin, and that LIS1 is essential for full complex assembly. The interaction between KASH5 and dynein is disrupted by mutation of the KASH5 EF hand domain, although dynein recruitment to KASH5 in cells is calcium independent. Since defective synapsis can lead to genetic abnormalities and infertility, the characterisation of the KASH5-dynein interaction is an important step forward in understanding the complex mechanism of chromosome movement during meiotic prophase I.

Results

KASH5 forms a complex with dynein, dynactin and LIS1

To investigate the interaction between dynein and KASH5 (Horn et al., 2013; Morimoto et al., 2012), we generated a stable HeLa cell line in which expression of GFP-KASH5 was induced by addition of doxycycline. This was used to examine the recruitment of endogenous dynein to the nuclei of KASH5-expressing cells by immunofluorescence. Since dynein requires the multi-subunit dynactin complex for function, we also probed for dynactin components. LIC1 and dynactin p50 were both recruited to KASH5-expressing nuclei (Fig. 1 A), in addition to dynactin p150 and IC (Horn et al., 2013). In contrast, neither dynein nor dynactin (Fig. 1 A) were recruited to the nuclei of cells transiently expressing a different KASH containing protein, nesprin-2α2 (GFP-N2α2).

We confirmed the recruitment of dynein and dynactin to KASH5 biochemically. HeLaM cells were transiently transfected with GFP-KASH5ΔK (Fig. 1 B) or GFP-N2α2ΔK, which lack their KASH and transmembrane domains, and so are cytosolic. LIC1, LIC2, IC and p150 all associated with GFP-KASH5ΔK and not with GFP-N2α2ΔK (Fig. 1 C). The KASH5 N-terminal 166 amino acids (GFP-KASH5ND), containing the EF-hands, were sufficient to pull down dynein IC and dynactin from cell lysates as efficiently as GFP-KASH5ΔK (Horn et al., 2013), and the same is true for LIC1 (Fig. 1 D).

LIS1 plays a key role in the assembly of DDA and D_2DA complexes (reviewed in (Canty and Yildiz, 2020; Markus et al., 2020; Olenick and Holzbaur, 2019), and co-precipitates with BICD2N along with dynein and dynactin (Splinter et al., 2012). In accordance with previous biochemical analysis (Horn et al., 2013), GFP-KASH5ΔK pulled down LIS1 as well as dynein and dynactin, but this complex excluded the dynein adaptor BICD2 (Fig. 1 C). Immunofluorescence analysis revealed that endogenous LIS1 was detected at the nuclear envelope in 99.8% of KASH5-expressing cells (Fig. S1 A), whereas the LIS1 and dynein interactor Nde1 was not, even though it could be detected at the nuclear envelope in late G2 cells (Fig. 1 A).

Hierarchy of dynein, dynactin and LIS1 recruitment to KASH5

We next sought to identify which dynein subunits mediate the KASH5 interaction, and the roles played by dynactin and LIS1. We used RNA interference to deplete individual dynein subunits in the GFP-KASH5 cell line (Fig. S2 A) and assessed the effect on recruitment to KASH5. Depletion of dynein IC2 (the only form expressed in HeLa cells: (Palmer et al., 2009)) did not prevent dynein recruitment (Fig. 2 A), with 100% of KASH5-positive nuclei being labelled with anti-LIC1 (Fig. S1 A). Cytosolic levels of LIC1 were reduced following IC2 depletion, making the nuclear envelope pool particularly distinct. This is likely due to a modest reduction in total dynein levels when IC2 is depleted, as seen by immunoblotting with anti-LIC1 and 2 (Fig. S2 A). LIS1 recruitment to KASH5 at the nuclear envelope was also unaffected by depletion of IC2 (Fig. 2 A and S1 B). Strikingly, dynactin was only rarely detected at the nuclear envelope in IC2-depleted cells using antibodies to p150 or p50 (Fig. 2 A and S2 A), even though p150 was still readily observed at microtubule plus ends. These data suggest that while the interaction between IC and p150 (Karki and Holzbaur, 1995; King

et al., 2003; Vaughan and Vallee, 1995) is not needed for dynein and LIS1 recruitment to KASH5, it is essential for the association of dynactin with KASH5.

Since IC2 depletion reduced total cellular dynactin p150 levels by ~25% (Fig. S1 A), we used a dominant negative approach as another way of testing the effect of disrupting IC2-p150 interactions on recruitment to KASH5, using over-expression of the coiled coil 1 region of p150 (CC1) (King et al., 2003; Quintyne et al., 1999). Because the stable GFP-KASH5 cell line was resistant to transient transfection, we co-transfected HeLa cells with GFP-KASH5 and myc-SUN2 (to ensure efficient localisation of KASH5 to the nuclear envelope) along with RFP-tagged CC1. Strikingly, while CC1 expression had no effect on dynein or LIS1 recruitment to KASH5, it prevented dynactin accumulation at the nuclear envelope (Fig. 2 B). These data confirm that dynein and LIS1 can associate with KASH5 independently of dynactin.

As the LICs have recently been recognised as having important interactions with cargo adaptors, we used RNAi to investigate their involvement in the dynein-KASH5 interaction. There was no reduction in the proportion of cells with detectable dynein, dynactin or LIS1 recruited to KASH5 after depleting LIC2 alone (Fig. 3 B, D). LIC1 depletion also had very little effect on dynactin or LIS1 recruitment in a binary scoring assay, but had a variable effect on dynein intermediate chain, with 80.8 ± 24.3% of cells (n=3 experiments, ±SD) showing IC signal at the nuclear envelope (Fig. 3 A, D). However, when both LIC1 and LIC2 were depleted simultaneously, the proportion of cells with detectable dynein and dynactin at the nuclear envelope was reduced by nearly 75% (Fig. 3 C, D). LIS1 recruitment was also reduced, but to a lesser extent than dynein or dynactin, with ~60% of KASH5 expressing cells showing LIS1 signal at the nuclear envelope. We were not able to deplete endogenous LIC1 completely using RNAi (Fig. S2 B) which may explain why in some cells a residual level of dynein, dynactin and LIS1 remained with KASH5 at the nuclear envelope. In addition, GFP-KASH5ΔK pull-downs from LIC1 and 2 depleted HeLa cells contained very little dynein and dynactin (Fig. 3 E). Thus, LIC1 and 2 act redundantly to recruit dynein and LIS1 to KASH5 at the nuclear envelope, with dynactin being recruited downstream, by a mechanism requiring the interaction between IC and p150.

We next used RNAi depletion of LIS1 in the GFP-KASH5 cell line to test if it is required for KASH5 to associate with dynein and dynactin. Interestingly, the proportion of cells with LIC1 detectable at the nuclear envelope was virtually unaffected by LIS1 knock-down (Fig. S1 C, D) whereas p150 recruitment was seen in only 20% of cells (Fig. S1 C, F). Dynein IC detection at KASH5-positive nuclei was highly variable between experiments (Fig. S1 C, E), with a mean of 57.1% of cells scoring positive for IC74 antibody labelling. The discrepancy between the anti-LIC1 and IC scoring most likely reflects the generally weaker nuclear envelope labelling seen with the IC74 antibody compared to anti-LIC1 antibodies in control cells. We interpret these data to mean that LIS1 depletion reduces dynein levels at the nuclear envelope somewhat, to levels that are still detectable by anti-LIC1 but sometimes not by IC74. Altogether, these data reveal that LIS1 is vital for the dynactin complex to be recruited to KASH5 downstream of dynein and suggest that LIS1 may also promote the formation of, or stabilise, the KASH5-dynein complex.

Dynein LIC1 residues 388-458 are essential for KASH5 binding and for dynein's function on multiple membrane cargoes

We next wanted to ascertain the LIC1 region responsible for the dynein-KASH5 interaction, focussing on the C-terminal domain that contains the cargo-binding helix 1 (residues 440-456) and helix 2 (residues 493-502) (Celestino et al., 2019; Lee et al., 2020; Lee et al., 2018). While helix 1 and some preceding amino acids (433-458) forms the minimal region needed for interaction with Hooks, BICD2 and Spindly (Lee et al., 2018), additional interactions between LIC1 and Spindly, BICD2 and Hook3 have been seen in helix 2 and the linker region upstream of helix 1 (Celestino et al., 2019). In contrast, RILP only requires helix 1 (LIC1 440-455) (Celestino et al., 2019). We generated a series of GFP-tagged human LIC1 constructs (Fig. 4 A): full length LIC1 (GFP-LIC1-FL: amino acids 1-523); a truncation which contains helix 1 but not helix 2 (GFP-LIC1-CT2: amino acids 1-456); and a construct which terminates shortly after the Ras-like domain and lacks both helix 1 and 2, as well as the linker sequences (GFP-LIC1-CT3: amino acids 1-388). We first examined the recruitment of the different LIC1 truncations to full length KASH5 at the nuclear envelope by immunofluorescence in HeLaM cells co-expressing HA-KASH5, myc-SUN2 and GFP-LIC1 constructs. Full-length GFP-LIC1 was efficiently recruited to KASH5, as expected (Fig. 4 B). The mid-length LIC1 CT2 construct was also strongly recruited to the nuclear envelope in

KASH5-SUN2 expressing cells. However, LIC1 1-388 (GFP-LIC1-CT3) was not recruited to KASH5 at all (Fig. 4 B). To verify these findings biochemically, cells depleted of LIC1 and 2 by RNAi were co-transfected with myc-tagged LIC1 truncations and the soluble GFP-KASHND construct. GFP trap immunoprecipitation revealed that while dynein containing FL-LIC1 and LIC1-CT2 was recruited to the KASH5 N-terminal domain, dynein with LIC1-CT3 was not (Fig. 4 C). These results indicate the LIC1 residues 388-456, containing helix 1 and its upstream linker sequence, are essential for the interaction with KASH5.

The importance of the LIC helix 1 in cargo binding prompted us to use these tools to assess the role of the LICs on a variety of endogenous membrane cargoes, for which the adaptors have not been fully defined (see discussion). First, we tested if LIC1 and 2 functioned redundantly in Golgi apparatus positioning, as there is conflicting evidence for the effects of depleting LICs on Golgi apparatus morphology and position (Kumari et al., 2021a; Palmer et al., 2009; Tan et al., 2011). RNAi depletion of LIC1 or 2 individually led to break-up of the Golgi ribbon in ~60% of HeLaM cells, with the Golgi fragments remaining centrally located (Fig. 5 A-C; Fig. S3 A). In contrast, depletion of both LICs simultaneously led to complete fragmentation and scattering of the Golgi apparatus (Fig. 5 B, C), suggesting that the LICs indeed act redundantly in Golgi positioning. This was confirmed by expressing RNAi-resistant LIC1-mKate or LIC2-mKate in cells depleted of both LICs (Fig. 5 D), as either LIC was able to fully restore Golgi apparatus clustering.

The endocytic pathway also relies heavily on dynein activity, which drives the movement of endocytic organelles towards the centrosome (Flores-Rodriguez et al., 2011; Granger et al., 2014; Reck-Peterson et al., 2018; Wang et al., 2019). This motility contributes to the sorting of endocytic cargo in the early endosome (Driskell et al., 2007). Depletion of both LICs profoundly altered the distribution of early endosomes, recycling endosomes and lysosomes (Fig. 6 A) while only minimal effects were seen with single depletions (not shown). Moreover, expression of either LIC1-mKate or LIC2-GFP restored the position of early endosomes, recycling endosomes and lysosomes (Fig. 6 B), confirming that LICs act redundantly in the general context of endocytic organelle motility, even though there are isoform-specific roles in SNX tubule dynamics (Hunt et al., 2013). We investigated if the same effects were observed with dynein recruitment to RILP. The presence of either LIC1 or

LIC2 was sufficient to recruit dynein and dynactin to HA-RILP-positive late endosomes, whereas recruitment of both complexes was significantly reduced when both LICs were depleted (Fig. S4 A-D).

To examine if the LIC1 region 388-456 that contains helix 1 is needed for Golgi apparatus positioning and in dynein's endocytic functions, we used the same knock-down and rescue approach (Figs. 5 E; 6 C, D; S4 E). Both the full length GFP-LIC1 and GFP-LIC1-CT2 rescued Golgi apparatus, early endosome, and lysosome clustering. In contrast, GFP-LIC1-CT3 did not restore retrograde transport, with EEA1-positive early endosomes (Fig. 6 C) and LAMP1-positive late endosomes/lysosomes (Fig. 6 D) remaining localised in the cell periphery, and the Golgi apparatus being fragmented and scattered (Fig. 5 E). Moreover, GFP-LIC1-CT3 did not interact with RILP, whereas GFP-LIC1-CT2 or full-length GFP-LIC1 were robustly recruited to RILP positive organelles (Fig. S4 E).

Altogether, these data provide clear *in cellulo* evidence that the LIC adaptor binding helix 1 is needed for dynein's interaction with KASH5 and RILP, and is also crucial for dynein's function on the Golgi apparatus, early endosomes and lysosomes. Furthermore, we demonstrate that LIC1 and LIC2 act redundantly in these situations.

KASH5 is a novel activating dynein adaptor

KASH5 shares key characteristics with other activating dynein adaptors: interaction with LIC helix 1; ability to recruit dynactin; and presence of an N-terminal dynein binding domain (containing EF-hands) followed by an extended coiled coil (Horn et al., 2013). In addition, KASH5's biological function in telomere clustering in prophase of meiosis I (Horn et al., 2013; Lee et al., 2015) strongly suggest that it recruits active dynein. When expressed out of its meiotic context, in HeLa cells, we quite often observed clusters of KASH5 and dynein around discrete points close to or on top of the nucleus (red arrowheads and arrows in Fig. 1 A), suggestive of clustering around the centrosome via active dynein. In addition, asymmetric distribution of KASH5 in the NE with enrichment towards the MTOC has been noted (Horn et al., 2013).

Overexpression of activating dynein adaptor proteins lacking their cargo binding domain disrupts dynein functions by sequestering dynein and preventing its binding to endogenous adaptors (e.g. (Hoogenraad et al., 2001; Hoogenraad et al., 2003; Horgan et al., 2010a; Horgan et al., 2010b; Splinter et al., 2012). As KASH5 demonstrates the characteristics of a cargo adaptor that interacts with LIC helix 1, we hypothesised that it would compete with other adaptors for binding to dynein. Indeed, overexpression of cytosolic GFP-KASH5ΔK in HeLaM cells resulted in complete fragmentation of the Golgi apparatus, and redistribution of lysosomes to the cell periphery; phenotypes indicative of a loss of dynein function (Fig. 7 A). In contrast, expression of a cytoplasmic KASH5 construct lacking its N terminal dynein binding domain (Fig. 1 B, GFP-KASH5ΔNDΔK (Horn et al., 2013)) had no effect on Golgi apparatus or lysosome distribution and morphology (Fig. 7 A). The effects of GFP-KASH5ΔK are therefore due to KASH5 binding and sequestering dynein, preventing its recruitment to other membrane cargoes. We also tested whether GFP-KASH5ΔK expression had dominant negative effects on spindle integrity in mitosis, since this is compromised in cells depleted of both LICs (Jones et al., 2014). Interestingly, neither GFP-KASH5ΔK nor GFP-KASH5ΔNDΔK expression affected bipolar spindle assembly (Fig. S5 A, B) whereas expression of mCherry-p50 caused profound defects leading to almost complete loss of bipolar spindles (Fig. S5 C). Furthermore, although BICD2N expression is highly disruptive for dynein's interphase function (Hoogenraad et al., 2001; Hoogenraad et al., 2003; Splinter et al., 2012), it had only minor effects on spindle assembly (Fig. S5 B). These data suggest that there may be cell cycle regulation of dynein adaptor binding.

We next determined if KASH5 competes with established dynein adaptors for dynein binding. To test this possibility, we co-transfected HeLaM cells with HA-tagged full-length KASH5, myc-tagged SUN2 and dominant negative versions of the activating adaptors BICD2 (GFP-BICD2N: (Hoogenraad et al., 2001; Splinter et al., 2012)) and Rab11-FIP3 (GFP-Rab11-FIP3 I737E, which retains its LIC binding domain but is unable to interact with Rab11 (Wilson et al., 2005)). Endogenous dynein was recruited to KASH5 at the nuclear envelope in control cells, but this was prevented when dominant negative dynein adaptors BICD2N and Rab11-FIP3 I737E were expressed (Fig. 7 B). We investigated if the same was true for dynein recruitment to RILP, even though RILP is not thought to be able to activate dynein/dynactin motility (Lee et al., 2020; Reck-Peterson et al., 2018). Dynein was recruited to RILP-positive

organelles following overexpression of HA-tagged RILP (Fig. 7 C). However, when GFP-BICD2N or GFP-Rab11-FIP3 I737E were co expressed, recruitment of dynein LIC1 to RILP was abrogated (Fig. 7 C). Taken together, these findings show that established dynein adaptor proteins compete with KASH5 and RILP for dynein binding.

To test directly if KASH5 could act as an activating adaptor and form motile complexes with dynein and dynactin, we used single molecule in vitro motility assays consisting of purified bacterially expressed KASH5 mixed with purified fluorescently-labelled dynein, dynactin and LIS1. We generated three KASH5 constructs encoding amino acids 1-407, 1-460, 1-507, all of which contain the N-terminal EF-hand dynein binding domain plus the predicted coiled coil region (amino acids 166-350), plus a variable amount of the C-terminal domain. SEC-MALS analysis showed that all three purified proteins formed dimers (shown for $KASH5_{1-460}$ in Fig. 8 B). Of these, $KASH5_{1-460}$ was the most active in preliminary motility assays. Purified dynein, dynactin and LIS1 alone displayed very little motility (Fig. 8 C). The inclusion of $KASH5_{1-460}$ promoted processive dynein movements (Fig. 8 D), although a lesser number than seen with purified $Hook3_{1-522}$ (Sf9/baculovirus expressed (Urnavicius et al., 2018)). Importantly, the velocity of processive dynein movements was the same for $KASH5_{1-460}$ and $Hook3_{1-522}$ (Fig. 8 E). KASH5, a transmembrane protein, is therefore a novel activating dynein adaptor.

KASH5's EF hand is critical for dynein and dynactin complex assembly

A common feature of several dynein adaptor proteins is the presence of an N terminal pair of EF hands in the dynein-binding domain, as seen in Rab11-FIP3, CRACR2a, Rab45/RASEF and ninein (Celestino et al., 2019; Lee et al., 2020; Reck-Peterson et al., 2018; Wang et al., 2019). KASH5 contains two putative EF hands, extending from amino acids 36-103, which form the bulk of the dynein binding domain (Fig. 1 B, D; 4 C). Sequence alignment of the KASH5 EF hands with CRACR2a, Rab45, FIP3 and ninein revealed that KASH5, like FIP3 and ninein, lacks some of the key consensus calcium-binding amino acids (at positions named X,Y,Z,-X,-Y,-Z), and that these changes were consistent across species (Fig. 9 A). EF hand 1 is particularly divergent, with only the residue in position X (Grabarek, 2006) matching the consensus, and with the key position -Z being a glutamine or histidine instead of a glutamate residue. While EF hand 2 has consensus amino acids in position X, other residues either do not conform or vary between species. For example, in non-rodent KASH5 EF hand

2, there is aspartate in place of glutamate at -Z, which can result in magnesium binding (Grabarek, 2006), as suggested for FIP3 (Lee et al., 2020).

This analysis suggested that KASH5 might not be calcium regulated. To determine if the KASH5 and Rab11-FIP3 interaction with dynein in cells required calcium or not, we expressed GFP-tagged KASH5 with myc-SUN2 in HeLaM cells, or GFP-Rab11-FIP3 in Vero cells, and labelled for endogenous LIC1. In control DMSO-treated cells there was robust recruitment of dynein to KASH5 at the nuclear envelope, and to Rab11-FIP3-positive recycling endosomes (Fig. S6). This recruitment was not affected by treating cells with the cell permeable calcium chelator, BAPTA-AM, for 2 hours to deplete intracellular calcium (Fig. S6). This demonstrates that the KASH5-dynein interaction does not require calcium and confirms that the Rab11-FIP3-dynein interaction in cells is calcium-independent, as reported for in vitro assays (Lee et al., 2020).

We wanted to test the importance of KASH5's EF hands in the dynein interaction, even if calcium was not required. The *fue* mutation in the zebrafish KASH5 homologue, futile cycle (fue) (Lindeman and Pelegri, 2012), gives zygotes are defective in pronuclear migration and mitotic spindle assembly (Dekens et al., 2003; Lindeman and Pelegri, 2012). The corresponding mutation in human KASH5 changes a valine to glutamic acid in EF hand 1 (V54E: Fig. 9 A). We generated KASH5-EF-*fue* constructs to establish how this mutation affected KASH5-dynein interactions. We also mutated the amino acids in positions X and Y of both EF hands to alanine (KASH5-EF-AA: D44A; Q46A; D81A; N83A: Fig. 9 A), based on similar mutations in CRACR2a which ablate its function (Srikanth et al., 2016; Wang et al., 2019). Lastly, we made two mutants where some KASH5 residues were replaced by those found in CRACR2a (Fig. 9 A). In KASH5-EF-mod1, four CRACR2a amino acid substitutions were made: Q46E; Q55D; P87Y and K88L. In KASH5-EF-mod2, nine amino acids in EF hands 1 and 2 and part of the exiting helix were changed to the CRACR2a sequences.

To test the effects of these mutations on KASH5 function, we harnessed the dominant negative effect of expressing cytosolic KASH5, which causes Golgi fragmentation and peripheral lysosome distribution (Fig. 5 and 6). In this assay, any mutant that prevents KASH5 from interacting with dynein would have no effect on organelle morphology when

459 expressed, as seen with GFP alone (Fig. 9 B). Overexpression of GFP-KASH5ΔK or GFP-
460 KASH5ΔK-mod1 in HeLaM cells resulted in complete fragmentation of the Golgi apparatus,
461 and peripheral lysosomes (Fig. 9 C, E, arrows). In contrast, GFP-KASHΔK-EF-*fue* (Fig. 9D),
462 GFP-KASHΔK-EF-AA (Fig. 9 F) or GFP-KASHΔK-EF-mod2 (Fig. 9 G) had no effect on Golgi
463 positioning or lysosome distribution, implying that these EF hand mutants were unable to
464 sequester dynein.
465
466 To validate these findings biochemically, we used GFP trap beads to isolate KASH5DK WT or
467 EF hand mutants from HeLaM cells, and then used antibodies directed against endogenous
468 IC and dynactin p150 to reveal which KASH5 constructs could form a stable complex with
469 dynein and dynactin. Unmodified GFP-KASH5ΔK co-precipitated with dynein and dynactin,
470 as did KASH5-mod1 (Fig. 9 H). However, the dynein and dynactin interaction was lost for the
471 KASH5-EF-*fue*, EF-AA, or EF-mod2 mutants. Taken together, these findings show that the
472 KASH5 EF hand is critical for its function with dynein and dynactin, although the interaction
473 is not calcium-dependent.
474
475
476 **Discussion**
477 Infertility will affect approximately 1 in 7 couples trying to conceive and has extraordinarily
478 detrimental effects on those affected. Despite this, surprisingly little is known about the
479 multitude of molecular and genetic causes of infertility in both males and females. This is
480 largely due to the complexity of meiosis, pronuclear migration, and a lack of samples to
481 study from sterile populations. Cytoplasmic dynein-1 is responsible for generating the
482 mechanical force required for the dynamic chromosome movements in meiotic prophase I,
483 which are essential for both meiotic progression and to maintain genetic integrity. KASH5,
484 the mammalian LINC complex component that spans the nuclear envelope, along with
485 SUN1/2, to link dynein to telomeres, is essential for synapsis and meiotic progression (Horn
486 et al., 2013; Morimoto et al., 2012). Here, we identify KASH5 as a novel activating adaptor
487 for dynein, the first trans-membrane protein with this role. We have mapped an important
488 dynein-KASH5 interaction domain and shown this to be the region (LIC1 residues 388-458)
489 containing the alpha-helix that mediates dynein's interaction with a plethora of other cargo
490 adaptor proteins (Celestino et al., 2019; Lee et al., 2020; Lee et al., 2018). As such, KASH5

competes with established dynein adaptors—BICD2 and FIP3—for dynein binding. Expression of a cytosolic truncation of KASH5 inhibits dynein interphase function (Fig. 7), as seen for other dynein adaptor constructs that cannot bind cargo (Hoogenraad et al., 2001; Hoogenraad et al., 2003; Horgan et al., 2010a; Horgan et al., 2010b; Splinter et al., 2012). Our *in vitro* assays (Fig. 8) confirm that KASH5 is an activating dynein adaptor (McKenney et al., 2014; Schlager et al., 2014a; Schlager et al., 2014b) as KASH5, in the presence of LIS1 and dynactin, promotes motility of purified dynein molecules (Fig. 8).

In vivo, however, KASH5-dynein-dynactin complexes will not be acting individually. It is estimated that there are ~80 LINC complexes per telomere (Spindler et al., 2019), providing an upper limit to the number of points where dynein motors can engage with the cytoplasmic face of the nuclear envelope. If KASH5 can bind more than one dynein motor per dynactin (Grotjahn et al., 2018; Urnavicius et al., 2018), then there could be 160 dyneins per telomere. It is obvious that considerable force must be exerted to move chromosomes around within the nucleoplasm to promote synapsis, and this could be provided by such an ensemble of dyneins. Importantly, we find that KASH5 recruits LIS1 as well as dynein and dynactin, and that LIS1 is needed for dynactin recruitment to KASH5. LIS1 is crucial for dynein function where high force is needed (Chapman et al., 2019; Markus et al., 2020; Pandey and Smith, 2011; Reddy et al., 2016; Yi et al., 2011), and has recently been shown to increase force generation of dynein-dynactin complexes in vitro by promoting the recruitment of two dynein motors per dynactin (Elshenawy et al., 2020; Htet et al., 2020; Markus et al., 2020).

LIS1 is thought to promote adaptor binding by opening the dynein phi complex to allow easier assembly of the dynein/dynactin/adaptor complex (Elshenawy et al., 2020; Gillies et al., 2022; Htet et al., 2020; Marzo et al., 2020; Qiu et al., 2019). Indeed, in cells, LIS1 enhances dynein and dynactin recruitment to a wide range of cellular cargoes (Cockell et al., 2004; Dix et al., 2013; Dzhindzhev et al., 2005; Lam et al., 2010; Siller et al., 2005; Sitaram et al., 2012; Splinter et al., 2012; Wang et al., 2013). Our data suggest that LIS1 is essential for recruiting dynactin to KASH5 (Fig. S1). Surprisingly, however, LIS1 depletion had much less effect on dynein recruitment. We also found that interfering with dynein IC-dynactin p150 interactions either by IC2 depletion or by over-expression of p150 CC1, did not prevent

dynein recruitment to KASH5. Based on these data, we propose that the first step in KASH5 adaptor complex assembly is an interaction between the LIC helix 1 and the adaptor. The subsequent binding of LIS1 then opens the Phi complex. The third step involves recruitment of the dynactin complex initiated by the IC-p150 interaction, followed by the formation of extensive contacts between the rest of the dynactin complex and the adaptor (Chowdhury et al., 2015; Grotjahn et al., 2018; Lau et al., 2021; Lee et al., 2020; Urnavicius et al., 2018; Urnavicius et al., 2015; Zhang et al., 2017). An interesting question is whether dynein's conformation (phi or open) affects its ability to bind adaptors, or subsequently recruit dynactin. If so, then LIS1 binding may regulate adaptor complex assembly *per se*. This KASH5 pathway contrasts with the association of dynein with the nuclear envelope at late G2/prophase, where the recruitment of dynein and dynactin are interdependent (Raaijmakers et al., 2013). The mechanism of dynein-dynactin-adaptor assembly may therefore depend on the adaptor and cellular context. While LIS1 does not remain in motile complexes with dynein and dynactin in vitro (Elshenawy et al., 2020; Htet et al., 2020), it appears to be a stable component of at least some DDA complexes in vivo because it is recruited to KASH5 at the nuclear envelope. It is also found along with dynein and dynactin in KASH5 (Fig. 1; (Horn et al., 2013)) and BICD2 pull-downs (Splinter et al., 2012). It is also required for dynein-dynactin recruitment to the nuclear envelope in late G2/prophase (Raaijmakers et al., 2013). Understanding fully the in vivo role of LIS1 in dynein-dynactin-adaptor function is a key challenge for the future.

KASH5 interacts with LICs via its N-terminal EF-hand domain, like the activating adaptors FIP3, CRACR2a, Rab45 and ninein (Celestino et al., 2019; Lee et al., 2020; Reck-Peterson et al., 2018; Wang et al., 2019). EF-hands are known for their regulation by calcium, and CRACR2a-dynein interactions are calcium-dependent (Wang et al., 2019). However, recent work has revealed that not all EF hand adaptors bind calcium, and calcium binding does not necessarily mean that the cellular function of the EF hand is regulated by calcium levels (Lee et al., 2020; Wang et al., 2019). Similarly, neither KASH5-dynein nor FIP3-dynein interactions were affected by depleting cells of calcium (Fig. S6), and the KASH5 EF-hands lack key residues known to be essential for calcium binding (Fig. 9 A). However, the structure of the KASH5 EF-hand is clearly vital, since mutating the X and Y positions of both EF-hands to alanine ablated KASH5-dynein interactions (Fig. 9). Similar adverse effects on dynein-KASH5

555 complex formation following mutation of other residues in KASH5 EF-hands have been
556 reported in a recent preprint (Agrawal et al., 2022). Importantly, our studies suggest why
557 the *fue* mutation in the EF-hand (Lindeman and Pelegri, 2012) is detrimental in zebrafish
558 development (Dekens et al., 2003; Lindeman and Pelegri, 2012), since replicating this
559 mutation in KASH5 also interferes with its ability to bind dynein. Interestingly, zebrafish *fue*
560 mutants are defective in pronuclear migration, despite a normal astral microtubule network
561 (Dekens et al., 2003). Similarly, Zyg12, the *C. elegans* LINC complex KASH-domain protein
562 that binds dynein LIC via a Hook domain, is needed for both pronuclear migration (Malone
563 et al., 2003; Minn et al., 2009) and meiotic synapsis (Sato et al., 2009). Whether KASH5 plays
564 a role in mammalian pro-nuclear migration remains to be determined.
565
566 As well as characterising KASH5 as a novel dynein activating adaptor, this study also
567 provides insight into LIC function in cells. RNAi depletion suggested that either LIC can
568 recruit dynein to KASH5 in cells (Fig. 3), and we have confirmed this using pull-downs with
569 GFP-LIC1 (Figs. 4, 9) and by reconstituting KASH5-activated motility of recombinant dynein
570 containing only LIC2 (Fig. 8). Similarly, we find that LICs 1 and 2 act redundantly for
571 recruitment of dynein to RILP, and in the positioning of the Golgi apparatus and recycling,
572 early and late endosomes in cells. We also show that the helix 1-containing region is
573 essential for all these roles. This is in keeping with roles for Hooks (Christensen et al., 2021)
574 and BicD2 (Hoogenraad et al., 2001; Hoogenraad et al., 2003; Splinter et al., 2012) at the
575 Golgi apparatus, and Hooks (Christensen et al., 2021; Guo et al., 2016; Olenick et al., 2019;
576 Villari et al., 2020), FIP3 (Horgan et al., 2010a; Horgan et al., 2010b) and RILP (Johansson et
577 al., 2007; Jordens et al., 2001; Scherer et al., 2014; Tan et al., 2011) in endocytic organelle
578 dynamics, since all of these adaptors can interact with both LICs (Celestino et al., 2019;
579 Christensen et al., 2021; Lee et al., 2020; Lee et al., 2018; Schlager et al., 2014a; Schroeder
580 et al., 2014; Schroeder and Vale, 2016; Urnavicius et al., 2018), although BicD2 may
581 preferentially bind LIC1 in vivo (Goncalves et al., 2019). It is important to remember,
582 however, that as yet there is no molecular explanation for why LIC1 is needed for motility of
583 SNX8-labelled endosomal tubules whereas LIC2-dynein moves SNX1 and SNX4 tubules (Hunt
584 et al., 2013).
585

Other isoform-specific roles for LICs have been described (see introduction), particularly in mitosis, where it has been proposed that LIC phosphorylation, coupled with Pin1 binding, may help control which adaptors bind to LIC1 and LIC2 during mitosis (Kumari et al., 2021a; Kumari et al., 2021b). LIC phosphorylation, notably in the region just upstream of helix 1, also plays a key role in switching dynein from interphase to mitotic cargos (Addinall et al., 2001; Dwivedi et al., 2019; Kumari et al., 2021a; Niclas et al., 1996). This may explain why KASH5 or BICD2N expression had little or no effect on mitotic spindle morphology (Fig. S5), even though they disrupt dynein's interphase functions. Phosphorylation of the adaptors themselves could potentially play a part in cell cycle control as well, since mitotic phosphorylation sites have been identified in, or close to, LIC binding domains in Hooks 1-3, BICD2 and FIP3 (Collins et al., 2012; Dephoure et al., 2008; Olsen et al., 2010; Wortzel et al., 2021). We can speculate that KASH5-LIC interactions, while vital in the prolonged prophase of meiosis I, would not be required, or could be detrimental, once cells enter pro-metaphase and throughout meiosis II. In support of this idea, we do not see accumulation of KASH5-containing membranes at mitotic spindle poles in our HeLa cell model. Cell cycle control of KASH5-LIC interactions will be a key area for future work.

Altogether, we have shown that KASH5 is a novel trans-membrane member of the dynein activating adaptor protein class, mapped its interaction with dynein LICs, and demonstrated that the KASH5 EF hands are critical for this process. This work also sheds light on order in which dynein-dynactin-adaptor complexes assemble in cells, and the involvement of LIS1 in this process.

Materials and Methods

Antibodies and constructs

The following mouse antibodies were used: dynein IC (IC74, MAB1618, Millipore; RRID:AB_2246059); EEA1 (Clone 14, BD Biosciences; RRID:AB_397830); LAMP1 (Clone H4A3, Developmental Studies Hybridoma Bank, RRID:AB_2296838; or Abcam, RRID:AB_470708); LIS1 (Sigma-Aldrich L7391; RRID:AB_260418); dynactin p150 (BD Transduction Laboratories 610473; RRID:AB_397845); GFP (Roche 11814460001; RRID:AB_390913); Myc-tag 9B11 (Cell signalling Technology 2276; RRID:AB_331783); GM130 (BD Transduction Laboratories 610822; RRID:AB_398141); transferrin receptor (Clone MEM-189, MA1-19300, ThermoFisher/Zymed; RRID:AB_2536952); and α-tubulin DM1A (Sigma-Aldrich T9026; RRID:AB_477593). The following rabbit antibodies were used: HA-tag (Sigma-Aldrich H6908; RRID:AB_260070); LAMP1 (Cell Signalling D2D11, monoclonal; RRID:AB_2687579); EEA1 (Cell Signalling Technology C45B10, monoclonal; RRID:AB_2096811); LIC1 (Cambridge Bioscience HPA035013, polyclonal; RRID:AB_10600807); LIC2 (Abcam ab178702, polyclonal); Nde1 (Proteintech, 10233-1-AP, polyclonal; RRID:AB_2149877). For Fig. 5 A, chicken anti-LIC1 and rabbit anti-LIC2 (Tan et al., 2011) were kindly provided by Prof. R. Vallee, Columbia University Medical Centre, USA. Secondary antibodies: Licor IRDye secondary antibodies (800CW or 680RD); Alexa Fluor 488, Alexa Fluor 594, Cy3, or Cy5 labelled donkey anti-mouse, -rabbit and -sheep (Jackson Immunoresearch).

Constructs

The following KASH5 constructs in pcDNA 4T/O have been previously described (Horn et al., 2013): GFP-KASH5; GFP-KASH5ΔK; GFP-KASH5ΔNDΔK; GFP-KASH5ΔCDΔK; GFP-KASH5ND, as has a myc-SUN2 construct in pcDNA3.1(-). EF-hand mutants were made using HiFi assembly (New England Biolabs) by linearising GFP-KASH5ΔK using Q5 polymerase with primers 5'GTCATGCGTGACTGGATTGCTG-3' and 5'-CGTGGAGTTGAGTATTTGCTCCTC-3' and inserting synthetic G-block sequences (Integrated DNA Technologies) encoding KASH5 bps 97-319 with the appropriate mutations (see Fig. 9). HA-KASH5ΔK was made by amplifying the KASH5ΔK sequence using forward primer 5'-GCGCGGATCCGACCTGCCCGAGGGCCC-3' and reverse primer 5'-GCGCGAATTCTTATGGATGTCGAGTGACTCTGAGC-3', digesting with BamH1 and EcoRI then ligating into pcDNA3.1 containing the HA tag sequence. For generating a stable cell line, full length GFP-KASH5 was inserted into the doxycyclin-inducible lentiviral

vector pTRIPZ (Open Biosystem, Singapore) after amplification using primers 5'-GCGCCTCGAGGACCTGCCCGAGGGCCCGGT-3' and 5'-GCGCACGCGTTCACACTGGAGGGGGCTGGAGG-3' followed by digestion with XhoI and MluI. Full length nesprin2α2 was amplified from a HeLa cDNA library and inserted into pcDNA3.1 downstream of GFP using XhoI and AflII digestion to give GFP-N2α2. A version lacking the transmembrane and KASH domain was generated in the same vector to give GFP-N2α2ΔK.

Silently-mutated siRNA resistant full length hLIC1-mKate, hLIC2-mKate and hLIC2-GFP have been previously described (Jones et al., 2014). RNAi-resistant full length LIC1 and LIC2 and LIC1 truncations were generated by PCR and restriction digest cloning into pEGFP-C3 (Clontech) and used for rescue experiments. GFP-LIC1-CT2 encodes amino acids 1-456 of human LIC1 with the addition of the amino acid sequence ADPPDLDN after the LIC1 C-terminus. GFP-LIC1-CT3 encodes amino acids 1-387 followed by ADPPDLDN. N-terminally Myc-tagged versions of full length human LIC1, LIC1-CT2 and LIC1-CT3 were generated using the forward primer 5'-CAGCTGGTACCGCGGCCGTGGGGCGAGTC-3'. The reverse primers were 5'-TCGAATCTAGACTAAGAAGCTTCTCCTTCCGTAGGAGATG-3' (full length LIC1), 5'-TCGAATCTAGACTAAGAGCCAGTCTTTTTACTCAACAAAC-3' (LIC1-CT2) and TCGAATCTAGACTATGGTGGTTGCTTTGCTAAAAGGGAC (LIC1-CT3), with no additional C-terminal amino acids. PCR products were inserted into pcDNA-3.1 downstream of a myc-tag sequence using KpnI and XbaI digestion.

Vectors encoding mCherry-chicken p50 and RFP-CC1 have been previously described (Wozniak et al., 2009). To generate GFP-BICD2N, the DNA sequence encoding amino acids 2-402 of mouse BICD2 was amplified using forward primer, 5'-GCGCGAATTCGTCGGCGCCGTCGGAGGAG-3'; reverse primer, 5'-GCGCGGATCCTCACAGGCGCCGCAGGGCACT-3', then cloned into pEGFP-C1 (Clontech) using EcoRI and BamHI. Other constructs were generous gifts from the following colleagues: pMDG2.1-VSV-G and p8.91-Gag-Pol vectors (Apolonia et al., 2015; Zufferey et al., 1997), Dr M. Malim (King's College London, UK); GFP-Rab11-FIP3 and GFP-Rab11-FIP3 I737E, (Wilson et al., 2005), Prof. G. Gould (University of Glasgow, UK); pEGFP-C1 containing hRILP (Colucci et al., 2005), Prof. Cecilia Bucci (University of Salento, Italy); pCB6-HA-RILP, Dr Mark Dodding (University of Bristol, UK).

672

673 **Cell lines and transfection**

674 HeLa and hTERT-RPE cells were obtained from ATCC; Vero cells were purchased from
675 European Collection of Authenticated Cell Cultures. HeLaM cells were kindly provided by Dr
676 Andrew Peden, University of Sheffield, UK. Mycoplasma testing was routinely performed by
677 DAPI staining.

678

679 HeLa, HeLaM, HEK293T and Vero cells were maintained in DMEM supplemented with 10%
680 FBS at 8.0% CO_2 and 37°C. To generate cells stably expressing human GFP-KASH5, HeLa cells
681 were transfected with pTRIPZ-GFP-KASH5, pMDG2.1-VSV-G and p8.91-GAG-POL in a ratio of
682 4:1:2 to a total of 10 µg of DNA using Lipofectamine 2000 (ThermoFisher) as per the
683 manufacturer's instructions overnight. Virus was then collected and passed through a 0.45
684 µm filter before addition to cells for 4 hours. Transduced cells were selected for with fresh
685 media containing puromycin (3µg/ml). Induction of GFP-KASH5 expression was induced with
686 doxycycline (500ng/ml) for 16 hours. Transient transfection of HeLaM and Vero cells on #1.5
687 coverslips was achieved using JetPEI (PolyPlus transfection), using half the manufacturer's
688 recommended amounts of total DNA and JetPEI. Expression levels were carefully titrated for
689 each plasmid, in some cases using dilution with carrier DNA (pBluescript SK-II) (Flores-
690 Rodriguez et al., 2011), to avoid over-expression artefacts. For biochemical analysis, cells
691 were transfected in 10 cm dishes using either JetPEI or PEI (Sigma 408727). PEI was
692 dissolved at 1 mg/ml in 150 mM NaCl by incubation at 50°C, sterile filtered and stored in
693 aliquots at -80°C. Per dish, 16 µg of total DNA was diluted in 200 µl Opti-MEM (Gibco
694 319850), 48 µl of PEI was added to another 200 µl Opti-MEM, then after 5 min the PEI was
695 added to the DNA mix and incubated for 30 min at room temperature before adding to the
696 cells.

697

698 **Short interfering RNA (siRNA) methods**

699 For depletion of target genes, siRNA transfections used INTERFERin (PolyPlus transfection).
700 siRNAs targeting the ORF of human LIC1 and LIC2 were obtained from Eurofins MWG
701 Operon. Oligonucleotides were applied to HeLaM cells at a final concentration of 5-20 nM
702 (for HeLaM) or 20 nM (for GFP-KASH5 HeLas) per target for 72 hours before analysis by
703 immunoblot and immunofluorescence. The following sequences were used, synthesised by

Eurofins MWG with dTdT overhangs: LIC1, 5'-AGAUGACAGUGUAGUUGUA-3'; LIC2, 5'-ACCUCGACUUGUUGUAUAA-3' (Jones et al., 2014; Palmer et al., 2009); LIS1, 5'-GAACAAGCGAUGCAUGAAG-3' (Lam et al., 2010; Tsai et al., 2005). For IC2, a SMARTpool (Thermo Scientific Dharmacon) was used consisting of a mixture of four siRNAs: 5'-GUAAAGCUUUGGACAACUA-3'; 5'-GAUGUUAUGUGGUCACCUA-3'; 5'-GCAUUUCUGUGGAGGGUAA-3'; 5'-GUGGUUAGUUGUUUGGAUU-3'. Control RNAi experiments were performed either using siGENOME lamin A/C Control (ThermoFisher Scientific: Fig. 5 A-C, 6 A, B) or ON-TARGET-plus Non-targeting siRNA #1 (Thermo Scientific Dharmacon).

For LIC rescue experiments analysed by immunofluorescence, cells were transfected with scrambled or LIC1 and LIC2 siRNAs for 48 h using INTERFERin (PolyPlus transfection), and then transfected in fresh media with siRNA-resistant GFP-LIC-FL, GFP-LIC1-CT2 or GFP-LIC1-CT3 using PEI or JetPEI (Fig. 4 C) with 72 hours total knock-down. In Fig. 3 E, LIC1 and 2-depleted cells were transfected after 48 hours with the indicated constructs using FuGENE6 and left for a further 24 hours.

Immunoblotting

For validating siRNA knock-down efficiency, lysates were collected 72 hours post siRNA addition in RIPA lysis buffer (Sigma-Aldrich R0278) supplemented with cOmplete ULTRA protease inhibitor (Roche 5892791001) and PhosSTOP (Roche PHOSS-RO) phosphatase inhibitor. A total of 20 µg of protein was loaded per well diluted in denaturing SDS loading buffer, and protein samples were separated using 12% polyacrylamide gels before being transferred to PVDF membranes. Membranes were blocked in 1x alpha-casein buffer (Sigma-Aldrich B6429) diluted in tris-buffered saline (TBS: 20 mM Tris/HCl, pH 7.7, 150 mM NaCl) for 1 hour at room temperature. Primary antibodies were diluted in 1x alpha-casein diluted in TBS supplemented with 0.01% Tween-20 (TBST) and incubated at 4°C overnight. Membranes were washed three times in TBST and incubated with Licor IRDye secondary antibodies (800CW or 680RD) diluted 1:10,000 in 1x alpha-casein in TBST for 1 hour at room temperature. Blots were washed three times in TBST and once in water before imaging on a Licor Odyssey or Odyssey CLx using Image Studio software.

736 **GFP-Trap immunoprecipitation**

737 For LIC truncation experiments, HeLaM cells were depleted of endogenous LIC1 and LIC2
738 and transiently transfected as described above. Cells were washed with ice cold PBS and
739 lysed in IP lysis buffer (50 mM Tris, pH 7.5, 10 mM NaCl, 2.5 mM $MgCl_2$, 1 mM DTT, 0.01%
740 digitonin [Calbiochem 300410] and protease inhibitors, 10 µg/ml aprotinin [Sigma A6103],
741 leupeptin [Calbiochem 108976] and pepstatin [Alfa Aesar J60237]) before centrifugation at
742 17,000 rpm for 30 mins at 4°C in a microcentrifuge. A tenth of the supernatant was taken as
743 an input sample, and the remaining supernatant was rotated at 4°C for 2 hours with
744 ChromoTek GFP-Trap® magnetic agarose beads pre-washed in IP wash buffer (50 mM Tris,
745 pH 7.5, 10 mM NaCl, 1 mM DTT and protease inhibitors). Beads were isolated and washed
746 three times in IP wash buffer and proteins eluted by boiling at 95°C in SDS-PAGE sample
747 buffer before analysis by SDS-PAGE and immunoblotting.
748
749 **BAPTA-AM treatment**
750 HeLaM cells were grown on uncoated #1.5 glass coverslips and Vero cells were grown on
751 coverslips coated with 1µg/ml Fibronectin (Sigma F0895). Cells were treated with either 10
752 µM BAPTA-AM (abcam ab120503) or DMSO vehicle control for 2 hours before fixation and
753 immunofluorescence labelling.
754
755 **Immunofluorescence**
756 HeLaM or Vero cells were grown on #1.5 coverslips at appropriate density. For EEA1
757 antibody labelling cells were fixed for 20 mins in 3% formaldehyde in PBS at RT. After
758 washing, unreacted formaldehyde was quenched with glycine (0.1 M) and permeabilised in
759 0.1% Triton X-100 in PBS for 10 mins before PBS wash prior to antibody labelling. For mitotic
760 spindle imaging, cells were fixed using formaldehyde/glutaraldehyde in a microtubule-
761 stabilising buffer containing 1% Triton-X100, as previously described in detail (Jones et al.,
762 2014). For all other antibody labelling, cells were fixed in methanol for 10 minutes at -20°C
763 and washed in PBS. Secondary antibodies labelled with Alexa Fluor 488, Alexa Fluor 594,
764 Cy3, or Cy5 were used along with 1 µg/ml DAPI, and samples were mounted in ProLong Gold
765 (Invitrogen). For LIS1 antibody labelling (Baffet et al., 2015), coverslips were washed once in
766 PBS then incubated for 1 min in PHEM buffer (60 mM PIPES, 25 mM HEPES, 10 mM EGTA,
767 2mM $MgCl_2$, pH 6.9) containing 0.5% Triton X-100. Cells were then transferred to PHEM

buffer supplemented with 3.7% paraformaldehyde for 20 minutes. This was followed by incubation in 0.2% Triton X-100 in PBS for 5 minutes. Coverslips were rinsed in PBS and quenched with glycine before labelling.

Imaging and analysis

Fixed HeLaM (Fig. 4; 5 E; 6 C, D; 7 B, C and 9) and Vero cells (Fig. S5 B) were imaged using an Olympus BX60 or BX50 microscope (Olympus Keymed) with a Plan apochromat 60X 1.4 N.A. oil immersion objective, CoolLED light source (CoolLED Ltd) or 100W Hg lamp, CoolSNAP ES CCD camera (Teledyne Photometrics) and MetaVue software (Molecular Devices). Subsequent image analysis was performed using MetaVue and ImageJ software. The imaging in Fig. 1-3, 5 A, 7 A and S4 A was performed on a IX71 microscope (Olympus) which was equipped for optical sectioning by a DeltaVision CORE system (GE Healthcare) with z-spacing fixed at 0.2 µm. Plan Apochromat 60X 1.4 N.A. or UPlanFl 100X 1.35 N.A. oil immersion objective lenses (Olympus) were used with a CoolSNAP HQ CCD camera (Photometrics). Deconvolution was completed using SoftWorX (Applied Precision) and images are displayed as z-projections.

Line scans were generated using Image J using the plot profile tool, with the lines starting in the cytoplasm. Data was exported and plotted as graphs in GraphPad Prism. ImageJ was used to generate inverted greyscale images, merge channels and draw cell outlines, using contrast-adjusted images as a guide, where needed. Some images were prepared and annotated using Adobe Photoshop. For phenotype scoring, each experiment was performed at least three times, and the number of cells manually scored are given in the Figure legends. Examples of the Golgi apparatus, early endosome and lysosome phenotypes are shown in Fig. S3. For dynein recruitment to KASH5 in Fig. 3 D and Fig. S2 D, cells were scored in a binary fashion as to whether dynein or dynactin could be seen at the nuclear envelope. For these data, statistical tests were not deemed appropriate as there was no variation in some control conditions, with all cells recruiting dynein/dynactin to KASH5. For other datasets, the statistical tests used are given in the figure legends. All analysis and graph preparation of statistics throughout this project was performed in GraphPad Prism 6 (GraphPad Software). For experiments where one condition was compared to a control an unpaired t-test was used. For experiments where multiple conditions were compared to one

control mean a one- or two-way ANOVA with Dunnett's post-hoc test were used. The p values are represented using the following method: p≤0.05=*, p≤0.01=**, p≤0.001=*** and p≤0.0001=****. Figures were assembled using Adobe Illustrator (Adobe) or Affinity Designer (Serif Europe Ltd).

Recombinant KASH5 protein expression and purification

Constructs of human KASH5 (amino acid residues: 1-407, 1-460 and 1-507) were cloned into pMAT11 vector (Peranen et al., 1996) for expression with N-terminal TEV-cleavable His_6-MBP tag. KASH5 constructs were expressed in BL21 (DE3) cells (Novagen), in 2xYT media, induced with 0.5 mM IPTG for 16 hr at 25°C. Bacterial pellets were harvested, resuspended in 20mM Tris pH 8.0, 500 mM KCl and lysed using a TS Cell Disruptor (Constant Systems) at 172 MPa. Cellular debris were later removed by centrifugation at 40,000 g. KASH5 fusion proteins were purified through consecutive Ni-NTA (Qiagen), amylose (NEB), and HiTrap Q HP (Cytiva) ion exchange chromatography. The N-terminal His_6-MBP tag was cleaved using TEV protease and the cleaved samples were further purified through HiTrap Q HP (Cytiva) ion exchange chromatography and size exclusion chromatography (HiLoad 16/600 Superdex 200, Cytiva) in 20 mM HEPES pH 7.5, 150 mM KCl, 2 mM DTT. Purified KASH5 protein samples were spin concentrated using Amicon® Ultra centrifugal filter device (10,000 NMWL), flash-frozen in liquid nitrogen and stored at -80°C. Purified KASH5 proteins were analysed using SDS-PAGE and visualised with Coomassie staining. Protein concentrations were determined using Cary 60 UV spectrophotometer (Agilent) with extinction coefficients and molecular weights calculated by ProtParam (http://web.expasy.org/protparam/).

Multi-angle light scattering coupled with size exclusion chromatography (SEC-MALS)

The absolute molar masses of KASH5 protein samples were determined by multi-angle light scattering coupled with size exclusion chromatography (SEC-MALS). KASH5 protein samples at > 1.5 mg ml^{-1} were loaded onto a Superdex™ 200 Increase 10/300 GL size exclusion chromatography column (Cytiva) in 20 mM Tris pH 8.0, 150 mM KCl, 2 mM DTT, at 0.5 ml min−1, in line with a DAWN® HELEOS™ II MALS detector (Wyatt Technology) and an Optilab® T-rEX™ differential refractometer (Wyatt Technology). Differential refractive index and light scattering data were collected and analysed using ASTRA® 6 software (Wyatt Technology). Molecular weights and estimated errors were calculated across eluted peaks

by extrapolation from Zimm plots using a dn/dc value of 0.1850 ml g^{-1}. Bovine serum albumin (ThermoFisher) was used as the calibration standard.

Protein purification

Full length human cytoplasmic dynein-1 (Schlager et al., 2014a) and human LIS1 (Baumbach et al., 2017) were expressed using the *Sf*9/baculovirus system and purified as previously described (Baumbach et al., 2017; Schlager et al., 2014a). Pellets from 1 L of Sf9 cell culture were suspended in 50 ml lysis buffer (50 mM HEPES pH 7.2, 100 mM NaCl, 1 mM DTT, 0.1 mM Mg.ATP, 10% Glycerol), supplemented with one cOmplete tablet (Roche) and 1mM PMSF. Cells were lysed using a Dounce homogeniser at 4°C, then lysate clarified for 45 mins at 500,000 x *g*. The supernatant was incubated with 1.5 ml pre-equilibrated IgG beads (Cytiva) for 3 h. Beads were washed with 200 ml lysis buffer. For dynein, beads were then transferred to a 2 ml tube, adding 10 µM SNAP-Cell TMR-Star dye (New England Biolabs) and incubating for 1 h at 4°C. Beads for both constructs were then washed with 100 ml TEV buffer (50 mM Tris-HCl pH 7.4, 148 mM K-acetate, 2 mM Mg-acetate, 1 mM EGTA, 10% Glycerol, 0.1 mM Mg.ATP, 1 mM DTT), then transferred again to a 2 ml tube, adding 400 µg TEV protease and incubating overnight at 4°C. Sample was then concentrated and gel filtered using a $G4000_{SWXL}$ 7.8/300 column (TOSOH Bioscience) into GF150 buffer (25 mM HEPES pH 7.2, 150 mM KCl, 1 mM $MgCl_2$, 5 mM DTT, 0.1 mM Mg.ATP) for dynein, or TEV buffer for Lis1. Peak fractions were concentrated and snap-frozen in liquid nitrogen.

Dynactin was purified from frozen porcine brains as previously described (Urnavicius et al., 2015). Porcine brains were blended with 300 ml homogenisation buffer (35 mM PIPES pH 7.2, 5 mM $MgSO_4$, 1 M KCl, 200 µM EGTA, 100 µM EDTA, 1 mM DTT) supplemented with four cOmplete tablets and 1mM PMSF until just thawed. The lysate was then clarified in two steps: 15 mins at 38,400 x *g* at 4°C, then 50 mins at 235,000 x *g* at 4°C. All subsequent steps were carried out at 4°C The supernatant was then filtered through a GF filter then a 0.45 µm filter, then loaded onto an SP Sepharose column (Cytiva), equilibrated with SP buffer A (35 mM PIPES pH 7.2, 5 mM $MgSO_4$, 1 mM EGTA, 0.5 mM EDTA, 1 mM DTT, 0.1 mM Mg.ATP). The resin was then washed until white using 99.5% SP buffer A/0.5% SP buffer B (35 mM PIPES pH 7.2, 5 mM $MgSO_4$, 1 M KCl, 1 mM EGTA, 0.5 mM EDTA, 1 mM DTT, 0.1 mM Mg.ATP), then dynactin was eluted using a gradient from 0.5-25% (% SP buffer B). Dynactin-

containing fractions were then filtered through a 0.22 µm filter, then loaded onto a Mono Q HR 16/60 column (Cytiva), pre-equilibrated with Mono Q buffer A (35 mM PIPES pH 7.2, 5 mM $MgSO_4$, 200 µM EGTA, 100 µM EDTA, 1 mM DTT). This column was washed with 10 CV Mono Q buffer A, then dynactin eluted using a 15-35% gradient (% Mono Q buffer B, 35 mM PIPES pH 7.2, 5 mM $MgSO_4$, 1 M KCl, 200 µM EGTA, 100 µM EDTA, 1 mM DTT). Peak fractions were concentrated and gel filtered using a $G4000_{SW}$ 21.5/600 column (TOSOH Bioscience) into GF150 buffer, with the peak concentrated and snap-frozen in liquid nitrogen.

Strep-tagged human Hook3 (1-522) (Urnavicius et al., 2018) was purified using the *Sf*9/baculovirus system as previously described (Urnavicius et al., 2018). A pellet from 500 ml of Sf9 culture was thawed using 50 ml Strep-tag lysis buffer (30 mM HEPES pH 7.2, 50 mM K-Acetate, 2 mM Mg-Acetate, 1 mM EGTA, 10% Glycerol, 1 mM DTT) plus one cOmplete tablet and 1 mM PMSF. Cells were then lysed using a Dounce homogeniser, with the lysate clarified for 20 minutes at 50,000 x *g* at 4°C. Supernatant was filtered using a GF filter, then flown onto a StrepTrap HP 1 ml column (Cytiva) at 4°C. Washed using 40 CV Strep-tag lysis buffer, then eluted with 3 mM desthiobiotin. Peak fractions were concentrated and gel filtered using a Superose 6 10/300 Increase column (Cytiva) into GF150 buffer. The monodisperse peak was concentrated and snap-frozen in liquid nitrogen.

in vitro TIRF motility assays

in vitro TIRF assays were carried out as previously (Urnavicius et al., 2018). Microtubules were typically prepared the day before the assay. Microtubules were made by mixing 1 µl of HiLyte Fluor 488 tubulin (2 mg/ml, Cytoskeleton), 2 µl biotinylated tubulin (2 mg/ml, Cytoskeleton) and 7 µl unlabelled pig tubulin (Schlager et al., 2014a) (6 mg/ml) in BRB80 buffer (80 mM PIPES pH 6.8, 1 mM $MgCl_2$, 1 mM EGTA, 1 mM DTT). 10 µl of polymerization buffer (2× BRB80 buffer, 20% (v/v) DMSO, 2 mM Mg.GTP) was added, then the solution was incubated at 37°C for 1 h for microtubule polymerization. The sample was diluted with 100 µl of MT buffer (BRB80 supplemented with 40 µM paclitaxel), then centrifuged at 21,000 x *g* for 9 minutes at room temperature to remove soluble tubulin. The resulting pellet was gently resuspended in 100 µl of MT buffer, then centrifuged again as above. 50 µl MT buffer was then added, with the microtubule solution then stored in a light-proof container. Before

usage, and every 5 hours during data collection, microtubule solution was spun again at 21,000 x *g* for 9 minutes, with the pellet resuspended in the equivalent amount of MT buffer.

Assay chambers were prepared by applying two strips of double-sided tape on a glass slide, creating a channel, then placing a piranha-solution-cleaned coverslip on top. The coverslip was then functionalized using PLL-PEG-Biotin (SuSOS), washed with 50 µl of TIRF buffer (30 mM HEPES pH 7.2, 5 $MgSO_4$, 1 mM EGTA, 2 mM DTT), then incubated with streptavidin (1 mg/ml, New England Biolabs). The chamber was again washed with TIRF buffer, then incubated with 10 µl of a fresh dilution of microtubules (2 µl of microtubules diluted into 10 µl TIRF-Casein buffer (TIRF buffer supplemented with 50 mM KCl and 1 mg/ml casein)) for 1 min. Chambers were then blocked with 50 µl blocking buffer.

Complexes were prepared mixing 1.5 µl of each component at the following concentrations: dynein at 0.3 µM, dynactin at 0.3 µM, adaptor at 6 µM, Lis1 at 50 µM. GF150 buffer was added to a final volume of 6 µl. Complexes were incubated on ice for 15 minutes then diluted with TIRF-Casein buffer to a final buffer of 15 µl. Four microliters of complex were added to 16 µl of TIRF-Casein buffer supplemented with an oxygen scavenging system (0.2 mg/ml catalase, Merck; 1.5 mg/ml glucose oxidase, Merck; 0.45% (w/v) glucose) 1% BME, 5 mM Mg.ATP. This mix was flown into the chamber.

The sample was imaged immediately at 23°C using a TIRF microscope (Nikon Eclipse Ti inverted microscope equipped with a Nikon 100x TIRF oil immersion objective). For each sample, a microtubule image was acquired using a 488 nm laser. Following this a 500-frame movie acquired (200 ms exposure, 4.1 fps) using a 561 nm laser. To analyse the data, ImageJ was used to generate kymographs from the tiff movie stacks. These kymographs were blinded, then events of similar length were picked to analyse velocity and number of processive events/µm microtubule/s, using criteria outlined previously (Schlager et al., 2014a; Urnavicius et al., 2018). Velocity was calculated using pixel size of 105 nm and frame rate of 235 ms/frame. Three replicates were taken for each sample, with velocities and number of processive events plotted using GraphPad Prism 7, using ANOVA with Tukey's multiple comparison to test significance.

928

929 **Supplementary material**

930 Fig. S1. demonstrates the effect of IC2 and LIS1 depletion on dynein and dynactin
931 recruitment to KASH5. It also provides an illustration of the meiotic LINC complex and the
932 role of dynein in meiotic prophase I. Fig. S2 shows immunoblot analysis demonstrating
933 depletion of targets by RNAi. Fig. S3 depicts Golgi apparatus, early endosome, and lysosome
934 phenotype categories used for the scoring shown in Figs. 5 and 6. Fig. S4 demonstrates that
935 LICs act redundantly to recruit dynein and dynactin to RILP-positive late endosomes, and
936 that dynein recruitment requires helix 1. Fig. S5 shows that the dominant negative
937 overexpression of KASH5 or BICD2N does not cause a major mitotic spindle assembly defect.
938 Fig. S6 depicts the effect of BAPTA-AM treatment on dynein recruitment to KASH5 and
939 Rab11-FIP3. Table S1 documents the full statistical analysis of the effects of LIC1 and LIC2
940 depletion on Golgi apparatus morphology shown in Fig. 5C.

941

942 **Acknowledgements**

943 The work in V. Allan's laboratory was funded by the Biotechnology and Biological Sciences
944 Research Council (BB/N006933/1 and a Ph.D. studentship to E. Granger), the Medical
945 Research Council (Ph.D. studentship to C. Villemant), and the University of Manchester. A.
946 Salter was funded by the University of Manchester-A*STAR Research Attachment
947 Programme (ARAP). We thank Mr Quentin Roebuck for excellent technical assistance. The
948 Bioimaging Facility microscopes used in this study were purchased with grants from BBSRC,
949 Wellcome and the University of Manchester Strategic Fund. We would like to thank Drs
950 Peter March and Graham Wright for their help with microscopy in Manchester and
951 Singapore, respectively. The work in B. Burke's laboratory was funded by the Singapore
952 Biomedical Research Council and the Singapore Agency for Science Technology and
953 Research, A*STAR. Funding for Singapore microscope? We are grateful to Dr Alessandra
954 Calvi for generating the nesprin2α construct. O. Davies is funded by a Wellcome Senior
955 Research Fellowship (Grant Number 219413/Z/19/Z). C. Lau is funded by grants from the
956 Wellcome Trust (WT210711) and the Medical Research Council, UK (MC_UP_A025_1011),
957 awarded to Dr. Andrew Carter. For the purpose of open access, the author has applied a CC
958 BY public copyright licence to any Author Accepted Manuscript version arising from this
959 submission.

960

961 The authors declare no competing financial interests.

962

963 **Author contributions**

964 Conceptualization: V. Allan, B. Burke. Funding acquisition: V. Allan, B. Burke. Designed and
965 performed experiments, and analysed data: A. Salter, K. Garner, V. Allan, C. Villemant, E.
966 Granger, M. Gurusaran, C. Lau, O. Davies. Generated molecular reagents: G. McNee, C.
967 Villement, A. Salter, V. Allan, E. Granger. Purified proteins: C. Lau, M. Gurusaran.
968 Supervision: V. Allan, B. Burke, P. Woodman, O. Davies. Visualization/data presentation: A.
969 Salter, K. Garner, V. Allan, C. Villemant, E. Granger, M. Gurusaran, C. Lau. Writing the initial
970 draft: A. Salter, K. Garner, V. Allan. Review & editing: all authors.

971

Figure legends

Figure 1. Recruitment of dynein, dynactin and LIS1 to KASH5 in HeLa cells.

(A) A stable HeLa cell line inducibly expressing GFP-KASH5 (green) was labelled with antibodies against dynein IC and LIC1, dynactin p150 and p50, LIS1 and Nde1 (magenta) and imaged on a DeltaVision microscope. Images are z-projections of deconvolved image stacks. The bottom panel shows the transient expression of GFP-N2α2 in green and labelling with anti-LIC1 in magenta, with undeconvolved wide-field images. Arrowheads point out the location of centrosomes, full arrows show creases in the nuclear envelope and asterisks mark cytoplasmic accumulations of GFP-KASH5. Thin white lines on colour merge images show where a line scan plot was performed, shown on the right. Scale bars = 10 µm. **(B)** Schematic showing KASH5 and the constructs used. For some experiments, the GFP was replaced with an HA tag. **(C)** Dynein, dynactin and LIS1 are recruited to KASH5 as shown by GFP-Trap pull-downs. HeLaM cells were transiently transfected with GFP-KASH5ΔK or GFP-N2α2ΔK. The pull-downs and inputs (1.5% of total lysate) were probed with antibodies against GFP, p150, IC, LIC1, LIC2, LIS1, BICD2 and α-tubulin. Molecular weight markers are shown. **(D)** The KASH5 N-terminal EF-hand domain is sufficient to recruit dynein. Lysates of HeLaM cells expressing GFP, GFP-KASH5ΔK (GFP-K5ΔK) or GFP-KASH5 N terminus (GFP-K5ND) were isolated by GFP-trap and probed for LIC1 by immunoblotting. The input is 15% of the GFP-trap sample.

Figure 2. Dynein and LIS1 recruitment to KASH5 does not require interaction between dynein IC and dynactin p150.

(A) HeLa cells stably expressing GFP-KASH5 (green) were depleted of IC2 using 20 nM siRNA for 72 hours and then processed for immunofluorescence with antibodies against LIC1, dynactin p150 and LIS1 (magenta). White lines on colour merge images show where a line scan plot was performed, shown on the right. **(B)** HeLa cells were transiently transfected with GFP-KASH5, RFP-CC1 and myc-SUN2 (CC1 and SUN2: not shown. Cells expressing CC1 are marked with asterisks). Cells were fixed and labelled with antibodies against dynein IC and LIC1, dynactin p50 and p150, and LIS1 (magenta in merges). Green lines on the GFP-KASH5 images indicate line scan locations, shown on the right. Images were taken on a

DeltaVision microscope and z-stack projections of deconvolved images are shown. Scale bars = 10 µm.

Figure 3. Dynein is recruited to KASH5 via either LIC1 or 2.

(A-D) HeLa cells stably expressing GFP-KASH5 (green) were depleted of LIC1 **(A)**, LIC2 **(B)**, or both LIC1 and 2 **(C)** using 10 nM of each siRNA for 72 hours, then fixed and labelled with antibodies against IC, dynactin p150 or LIS1 (magenta). Thin white lines show where a line scan plot was performed on LIC1&2 depleted cells, shown on the right. Images were taken on a DeltaVision microscope and z-stack projections of deconvolved images are shown. Scale bars = 10 µm. **(D)** LIC depleted cells were scored in a binary fashion for recruitment of IC, p150 or LIS1 to KASH5. The mean and standard deviation of each condition is shown. The experiment was repeated three times, with 300 cells scored for each condition in each experiment. **(E)** HeLaM cells were depleted with siRNA against both LICs together (10 nM each), or with control siRNAs. 48 hours into the knockdown, cells were transfected with either GFP-KASH5ΔK or GFP-N2α2ΔK. The following day cells were lysed and a GFP trap was performed. Input and pull-downs were immunoblotted with antibodies against GFP, p150, LIC1, LIC2, IC and α-tubulin. The input was 1.5% of the total cell lysate. Molecular weight markers are shown on the right.

Figure 4. KASH5-LIC1 interactions require LIC1 helix 1.

(A) Schematic of LIC1 showing the N terminal GTPase-like domain that is highly conserved between LIC1 and LIC2, and a less well conserved C terminal domain containing two alpha-helices termed Helix 1 (440-456) and Helix 2 (493-502). Truncated versions of LIC1 were generated that lacked Helix 2 (LIC1 CT2) or both Helix 1 and Helix 2 (LIC1 CT3). **(B)** HeLaM cells were depleted of LIC1 and 2 using 5 nM of each siRNA for 48 hours. GFP-tagged LIC truncation constructs were co-transfected with full-length HA-tagged KASH5 (and myc-SUN2: not shown) for a further 24 hours, then fixed and labelled with antibodies to HA (magenta) and imaged by wide-field microscopy. Scale bars = 10 µm. **(C)** HeLaM cells were depleted of both LICs by siRNAs for 48 hours, then co-transfected with Myc-tagged LIC1 constructs and GFP-KASH5ND or GFP as a control, and incubated for a further 24 hours. Cell lysates were incubated with GFP-trap beads then analysed by SDS-PAGE and

immunoblotting with antibodies to GFP, myc and IC (IC74) to detect native dynein. The input is 15% of the GFP-trap sample.

Figure 5. LICs 1 and 2 act redundantly in Golgi apparatus positioning, with helix 1 being essential.

(A-C) HeLaM cells were depleted of LIC1, LIC2 or both LICs using 5 nM siRNA for each subunit, then analysed by immunoblotting of lysates with antibodies to LIC1 and 2 (Tan et al., 2011) **(A)**, or fixed and labelled with antibodies to GM130 and imaged on a DeltaVision microscope to reveal the Golgi apparatus **(B)**. Z-projections of deconvolved images stacks are shown. **(C)** Golgi morphology was scored manually as shown in Fig. S3 for 100 cells per condition, in 3 independent experiments. Statistical analysis was performed using two-way ANOVA with Tukey's test (see Table S1 for complete results): comparisons vs. control samples are shown on the graph ($p \leq 0.01$=**, $p \leq 0.0001$=****). **(D, E)** HeLaM cells were depleted of both LICs then transfected with RNAi-resistant LIC1-mKate or LIC2-mKate **(D)** or GFP-LIC1-FL, GFP-LIC1-CT2, GFP-LIC1-CT3 and GFP constructs **(E)**. GM130 labelling was used to reveal Golgi apparatus morphology (wide-field images: asterisks mark cells expressing the constructs). Golgi morphology was scored for ~100 cells per experimental condition in three independent experiments **(E)**. All scale bars = 10 µm.

Figure 6. LICs 1 and 2 act redundantly in endocytic organelle positioning, with helix 1 being essential.

(A) HeLaM cells were depleted of Lamin A/C or LIC 1 and 2 using 5 nM of each siRNA duplex and stained for organelle markers (EEA1, early endosomes; LAMP1, lysosomes; TfR, recycling endosomes). **(B)** LIC-depleted cells were transfected with siRNA-resistant LIC1-mKate or LIC2-GFP and antibody labelled. The boxed region in the LAMP1 image is shown at two different focal planes. Asterisks mark transfected cells. **(C, D)** LIC depleted cells were transfected with GFP-LIC1 FL, CT2, CT3 or GFP. Asterisks mark transfected cells. Control knockdown cells were not transfected. Cells were labelled with anti-EEA1 **(C)** or anti-LAMP1 **(D)**. All images are wide-field. Scale bars = 10 µm. Early endosome and lysosome position phenotypes were scored as outlined in Fig. S3, with ~100 cells per condition, repeated in 3 independent experiments.

Figure 7. KASH5 has properties of a dynein adaptor.

(A) HeLaM cells transiently expressing GFP-KASH5ΔK or GFP-KASH5ΔNΔK (which lacks the dynein binding domain) were labelled with GM130 or LAMP1 antibodies (z-stack projections of deconvolved images shown). Cells were scored for phenotypes associated with dynein inhibition: Golgi apparatus scattering, peripheral clustering of lysosomes and enlarged lysosomes. Manual scoring of 100 cells per condition was repeated in three independent experiments, with mean and S.D. shown. An unpaired t-test was performed comparing GFP-KASH5ΔK- and GFP-KASH5ΔNΔK- expressing cells for each phenotype. **** = p≤0.0001, *** = p≤0.001, ** = p≤0.01. **(B, C)** Full length HA-KASH5 **(B)** or HA-RILP **(C)** were expressed alone (top panel, control) or with dominant negative GFP-BICD2N (middle panel), or dominant negative GFP-Rab11-FIP3-I73E (bottom panel) in HeLaM cells. Endogenous dynein was visualised along with HA-KASH5 or HA-RILP using antibodies to LIC1 and HA (wide-field imaging, scale bar = 10 µm). Thin black and white (left panels) or red lines (LIC1 panels) show where line scan plots were performed (right).

Figure 8. KASH5 is an activating adaptor for dynein motility in vitro.

(A) SDS-PAGE and Coomassie blue staining of purified bacterially-expressed $KASH5_{1\text{-}406}$. **(B)** SEC-MALS analysis of $KASH5_{1\text{-}460}$ demonstrating a molecular weight of 101 kDa (predicted dimer molecular weight is 103 kDa). **(C)** Purified baculovirus-expressed recombinant dynein, LIS1 and porcine brain dynactin were combined with and without $KASH5_{1\text{-}460}$ and motility of individual 6-carboxytetramethylrhodamine-labelled dynein molecules was visualised using TIRF microscopy. The activating adaptor $Hook3_{1\text{-}522}$ was used as a positive control. **(D)** The number of processive events per µm microtubule per minute was determined from kymographs in a blinded fashion for all three conditions in three technical replicates, with the mean ± S.D. plotted. The total number of movements analysed were 2066 for Hook3, 339 for KASH5 and 34 for the no addition control. Significance was determined using ANOVA with Tukey's multiple comparison (ns = not significant, * = p≤0.05, **** = p≤0.0001). **(E)** The mean velocity of processive dynein movements from the $KASH5_{1\text{-}406}$ and $Hook3_{1\text{-}522}$ data are plotted (± S.D., n=3 replicates).

Figure 9. KASH5's EF hand is critical for dynein and dynactin complex assembly.

(A) Top: Sequence comparison between human KASH5 and other dynein adaptors containing EF-hands, and between KASH5 proteins from different species. The EF-hand consensus sequence is shown, along with position nomenclature (Grabarek, 2006). Bottom: mutations generated in KASH5 EF-hands (altered amino acids shown in red), along with published mutations in the calcium-dependent dynein adaptor CRACR2a (Wang et al., 2019). KASH5 mutant dynein-binding activity is indicated by + or - symbols. **(B-G)** GFP-tagged KASH5ΔK, GFP-KASHΔK EF-hand mutants, or GFP were expressed in HeLaM cells. Cells were then fixed and labelled with antibodies to GFP (shown in magenta), GM130 (yellow) and LAMP1 (cyan) to test if the expressed protein disrupted endogenous dynein function. Arrows in merged panels indicate peripheral clusters of lysosomes. Wide-field imaging; scale bar = 10 µm. **(H)** GFP-trap immunoprecipitates from cells expressing the GFP-hKASH5ΔK EF hand mutants, or GFP-hKASH5ΔK probed with antibodies to GFP, dynein IC and dynactin p150.

Supplementary Figure 1. Effect of IC2 and LIS1 depletion on dynein and dynactin recruitment to KASH5.

(A) Illustration depicting how the meiotic LINC complex connects telomeres inside the nucleus to cytoplasmic dynein in the cytoplasm. Dynein movement begins to drag the telomeres towards the centrosome (yellow dots) in leptotene of prophase I, leading to the formation of the chromosome 'bouquet' in zygotene. This movement allows pairing of homologous chromosomes and the formation of the synaptonemal complex. INM, inner nuclear membrane; ONM, outer nuclear membrane. **(B)** HeLa cells stably expressing GFP-KASH5 (green) were depleted of IC2 using 20 nM siRNA for 72 hours and then processed for immunofluorescence with antibodies against LIC1, dynactin p150 and LIS1. Cells were scored in a binary fashion for recruitment IC, LIC1 or p150 to KASH5. The mean and standard deviation is shown for three independent repeats in which 300 cells were scored for each condition. **(C-F)** HeLa cells stably expressing inducible GFP-KASH5 were depleted of LIS1 using 20 nM siRNA, induced to express GFP-KASH5 and then fixed and labelled. **(C)** Cells were scored in a binary fashion to determine if cells showed recruitment IC, LIC1 or p150 to KASH5. The mean and standard deviation is shown for four independent repeats in which 300 cells were scored for each condition. Statistical tests were determined as not being appropriate for the data in B or C, as there is no variation in some control conditions.

Immunofluorescence images showing GFP-KASH5 in green and antibodies against dynein LIC1 **(D)**, IC **(E)** and dynactin p150 **(F)** in magenta. Images were taken on a DeltaVision microscope followed by deconvolution. Images are Z-stack projections. Thin white lines on colour images are site of line scans which are shown on the right. Scale bar represents 10 µm.

Supplementary Figure 2. Immunoblot analysis demonstrating depletion of targets by RNAi.

(A) HeLa cells stably expressing inducible GFP-KASH5 were depleted of various dynein subunits or LIS1 using 20 nM siRNAs against the following targets: Control (Sc), LIC1, LIC2, LIC1&2, IC2 and LIS1. Representative western blots of cell lysates of knockdown cells are shown. Blots were probed with antibodies against GFP, p150, IC, LIC1, LIC2, LIS1 and α-tubulin followed by fluorescently-labelled secondary antibodies. Molecular weight markers are shown on the right of the blots. The efficiency of knockdowns was analysed by quantification of blots using Image Studio software, with correction for protein loading using the anti-tubulin signal. Experiments were repeated four times alongside immunofluorescence experiments. Error bars represent standard deviations. **(B)** Immunoblotting of HeLaM cells depleted with 5 nM each of LIC1 and LIC2 duplexes, or 20 nM control duplexes, for 72 hours. Blots were probed with antibodies to dynein LIC1, LIC2, IC (IC74) and dynactin p150.

Supplementary Figure 3. Depiction of Golgi apparatus, early endosome, and lysosome phenotype categories.

HeLaM cells were treated with 5 nM LIC1 plus 5 nM LIC2 for 72 hours in total. Cells were fixed after 72 hours and processed for immunofluorescence with antibodies to GM130 (Golgi apparatus), EEA1 (early endosomes) or LAMP1 (lysosomes) and example images of each phenotype collected. A schematic drawing of each category is shown, with representative cells for that category indicated by asterisks in the immunofluorescence panel.

Supplementary Figure 4. LICs act redundantly to recruit dynein and dynactin to RILP-positive late endosomes, and recruitment requires helix 1.

(A-D) Cells were depleted of LICs individually or together for 48 hours using a total of 20 nM siRNA then transfected with GFP-RILP and fixed 1 day later and labelled for IC **(A)** or dynactin p150 **(B)**. Control cells (not siRNA treated) were transfected with GFP-RILP. DeltaVision deconvolved images are shown as z-stack projections. Scale bar = 10 µm. The percentage of cells with GFP-RILP structures labelled with IC **(C)** or p150 **(D)** was scored (± S.D.). At least 100 cells were scored in each of three independent experiments. *** = P<0.001, **** = P<0.0001, one-way ANOVA with Dunnett's post-hoc test. **(E)** HeLaM cells were co-transfected with HA-RILP and GFP-LIC1 full length, CT2 or CT3. Wide-field images are shown; scale bar = 10 µm.

Supplementary Figure 5. The dominant negative overexpression of KASH5 or BICD2N does not cause a major mitotic spindle assembly defect.

HeLaM cells were transfected with **(A)** GFP-KASH5ΔNΔK, **(B)** GFP-KASH5ΔK, **(C)** GFP-BICD2-N or **(D)** mcherry-P50. They were fixed using a protocol to maintain mitotic cells on the coverslips (fix-perm: see methods) and then labelled with antibodies against α-tubulin and pericentrin. Images were taken on a DeltaVision microscope followed by deconvolution. Z-stack projections are shown. Scale bar is 10 µm. **(E)** Mitotic HeLaM cells that were untransfected or transiently expressing the indicated construct were scored depending on whether the spindle was bipolar or disrupted. The experiment was repeated three times and 100 cells scored in each condition, and the mean and S.D. are shown. * = p≤0.05, *** = p≤0.001, one-way ANOVA with Dunnett's post-hoc test.

Supplementary Figure 6. Effect of BAPTA-AM treatment on dynein recruitment to KASH5 and Rab11-FIP3.

Following transient transfection of HeLa M cells with GFP-KASH5-FL **(A)** or Vero cells with GFP-Rab11-FIP3 **(B)**, cells were treated with either DMSO vehicle control or 10 µM BAPTA-AM for 2 hours at 37°C. Cells were fixed and labelled with antibodies to endogenous LIC1 and epitope tags. Wide-field images, with boxed regions shown as enlargements in **(B)**. Scale bar represents 10 µm.

Table S1. Statistical analysis of the effects of LIC1 and LIC2 depletion on Golgi apparatus morphology.

1194 The data presented graphically in Figure 5C were analysed by Two-way ANOVA with Tukey's
1195 test. P values: ** ≤ 0.01, **** ≤ 0.0001. Analysis of 100 cells per condition, in each of 3
1196 independent experiments.

References

Addinall, S., P. Mayr, S. Doyle, J. Sheehan, P. Woodman, and V. Allan. 2001. Phosphorylation by cdc2-cyclinB1 kinase releases cytoplasmic dynein from membranes. *J. Biol. Chem.* 276:15939-15944.

Agrawal, R., J.P. Gillies, J. Zang, J. Zhang, S. Garrott, H. Shibuya, J. Nandakumar, and M.E. DeSantis. 2022. The KASH5 protein involved in meiotic chromosomal movements is a novel dynein activating adaptor. *bioRxiv*. doi.org/10.1101/2022.03.11.483947:Posted March 12, 2022.

Apolonia, L., R. Schulz, T. Curk, P. Rocha, C.M. Swanson, T. Schaller, J. Ule, and M.H. Malim. 2015. Promiscuous RNA binding ensures effective encapsidation of APOBEC3 proteins by HIV-1. *PLoS Pathog*. 11:e1004609.

Baffet, A.D., D.J. Hu, and R.B. Vallee. 2015. Cdk1 Activates Pre-mitotic Nuclear Envelope Dynein Recruitment and Apical Nuclear Migration in Neural Stem Cells. *Dev Cell*. 33:703-716.

Baumbach, J., A. Murthy, M.A. McClintock, C.I. Dix, R. Zalyte, H.T. Hoang, and S.L. Bullock. 2017. Lissencephaly-1 is a context-dependent regulator of the human dynein complex. *Elife*. 6.

Belyy, V., M.A. Schlager, H. Foster, A.E. Reimer, A.P. Carter, and A. Yildiz. 2016. The mammalian dynein-dynactin complex is a strong opponent to kinesin in a tug-of-war competition. *Nat Cell Biol*. 18:1018-1024.

Bentebbal, S.A., B.R. Meqbel, A. Salter, V. Allan, B. Burke, and H.F. Horn. 2021. A human infertility-associated KASH5 variant promotes mitochondrial localization. *Sci Rep*. 11:10133.

Bielli, A., P.-O. Thörnqvist, A. Hendrick, R. Finn, K. Fitzgerald, and M. McCaffrey. 2001. The small GTPase Rab4A interacts with the central region of cytoplasmic dynein light intermediate chain-1. *Biochem. Biophys. Res. Comm.* 281:1141-1153.

Bone, C.R., and D.A. Starr. 2016. Nuclear migration events throughout development. *J Cell Sci*. 129:1951-1961.

Burke, B. 2018. LINC complexes as regulators of meiosis. *Curr Opin Cell Biol*. 52:22-29.

Canty, J.T., and A. Yildiz. 2020. Activation and Regulation of Cytoplasmic Dynein. *Trends Biochem Sci*. 45:440-453.

1228 Celestino, R., M.A. Henen, J.B. Gama, C. Carvalho, M. McCabe, D.J. Barbosa, A. Born, P.J.
1229 Nichols, A.X. Carvalho, R. Gassmann, and B. Vogeli. 2019. A transient helix in the
1230 disordered region of dynein light intermediate chain links the motor to structurally
1231 diverse adaptors for cargo transport. *PLoS Biol*. 17:e3000100.
1232 Chapman, D.E., B.J.N. Reddy, B. Huy, M.J. Bovyn, S.J.S. Cruz, Z.M. Al-Shammari, H. Han, W.
1233 Wang, D.S. Smith, and S.P. Gross. 2019. Regulation of in vivo dynein force production
1234 by CDK5 and 14-3-3epsilon and KIAA0528. *Nat Commun*. 10:228.
1235 Chikashige, Y., C. Tsutsumi, M. Yamane, K. Okamasa, T. Haraguchi, and Y. Hiraoka. 2006.
1236 Meiotic proteins bqt1 and bqt2 tether telomeres to form the bouquet arrangement
1237 of chromosomes. *Cell*. 125:59-69.
1238 Chowdhury, S., S.A. Ketcham, T.A. Schroer, and G.C. Lander. 2015. Structural organization of
1239 the dynein-dynactin complex bound to microtubules. *Nat. Struct. Mol. Biol.* 22:345-
1240 347.
1241 Christensen, J.R., A.A. Kendrick, J.B. Truong, A. Aguilar-Maldonado, V. Adani, M.
1242 Dzieciatkowska, and S.L. Reck-Peterson. 2021. Cytoplasmic dynein-1 cargo diversity is
1243 mediated by the combinatorial assembly of FTS-Hook-FHIP complexes. *Elife*. 10.
1244 Cockell, M.M., K. Baumer, and P. Gonczy. 2004. lis-1 is required for dynein-dependent cell
1245 division processes in C. elegans embryos. *J Cell Sci*. 117:4571-4582.
1246 Collins, L.L., G. Simon, J. Matheson, C. Wu, M.C. Miller, T. Otani, X. Yu, S. Hayashi, R. Prekeris,
1247 and G.W. Gould. 2012. Rab11-FIP3 is a cell cycle-regulated phosphoprotein. *BMC Cell*
1248 *Biol*. 13:4.
1249 Colucci, A.M., M.C. Campana, M. Bellopede, and C. Bucci. 2005. The Rab-interacting lysosomal
1250 protein, a Rab7 and Rab34 effector, is capable of self-interaction. *Biochemical and*
1251 *biophysical research communications*. 334:128-133.
1252 Dekens, M.P.S., F.J. Pelegri, H.-M. Maischein, and C. Nüsslein-Volhard. 2003. The maternal-
1253 effect gene futile cycle is essential for pronuclear congression and mitotic spindle
1254 assembly in the zebrafish zygote. *Development*. 130:3907-3916.
1255 Dephoure, N., C. Zhou, J. Villen, S.A. Beausoleil, C.E. Bakalarski, S.J. Elledge, and S.P. Gygi.
1256 2008. A quantitative atlas of mitotic phosphorylation. *Proc Natl Acad Sci U S A*.
1257 105:10762-10767.
1258 Ding, X., R. Xu, J. Yu, T. Xu, Y. Zhuang, and M. Han. 2007. SUN1 is required for telomere
1259 attachment to nuclear envelope and gametogenesis in mice. *Dev Cell*. 12:863-872.

Dix, C., H. Soundararajan, N. Dzhindzhev, F. Begum, B. Suter, H. Ohkura, E. Stephens, and S. Bullock. 2013. Lissencephaly-1 promotes the recruitment of dynein and dynactin to transported mRNAs. *J. Cell Biol.* 202:479-494.

Driskell, O., A. Mironov, V. Allan, and P. Woodman. 2007. Dynein is required for receptor sorting and the morphogenesis of early endosomes. *Nat Cell Biol*. 9:113-120.

Dunce, J.M., A.E. Milburn, M. Gurusaran, I. da Cruz, L.T. Sen, R. Benavente, and O.R. Davies. 2018. Structural basis of meiotic telomere attachment to the nuclear envelope by MAJIN-TERB2-TERB1. *Nat Commun*. 9:5355.

Dwivedi, D., A. Kumari, S. Rathi, S.V.S. Mylavarapu, and M. Sharma. 2019. The dynein adaptor Hook2 plays essential roles in mitotic progression and cytokinesis. *J Cell Biol*. 218:871-894.

Dzhindzhev, N.S., S.L. Rogers, R.D. Vale, and H. Ohkura. 2005. Distinct mechanisms govern the localisation of Drosophila CLIP-190 to unattached kinetochores and microtubule plus-ends. *J Cell Sci*. 118:3781-3790.

Elshenawy, M.M., J.T. Canty, L. Oster, L.S. Ferro, Z. Zhou, S.C. Blanchard, and A. Yildiz. 2019. Cargo adaptors regulate stepping and force generation of mammalian dynein-dynactin. *Nat Chem Biol*. 15:1093-1101.

Elshenawy, M.M., E. Kusakci, S. Volz, J. Baumbach, S.L. Bullock, and A. Yildiz. 2020. Lis1 activates dynein motility by modulating its pairing with dynactin. *Nat Cell Biol*. 22:570-578.

Even, I., S. Reidenbach, T. Schlechter, N. Berns, R. Herold, W. Roth, D. Krunic, V. Riechmann, and I. Hofmann. 2019. DLIC1, but not DLIC2, is upregulated in colon cancer and this contributes to proliferative overgrowth and migratory characteristics of cancer cells. *FEBS J*. 286:803-820.

Feng, Q., A.M. Gicking, and W.O. Hancock. 2020. Dynactin p150 promotes processive motility of DDB complexes by minimizing diffusional behavior of dynein. *Mol Biol Cell*. 31:782-792.

Fenton, A.R., T.A. Jongens, and E.L.F. Holzbaur. 2021. Mitochondrial adaptor TRAK2 activates and functionally links opposing kinesin and dynein motors. *Nat Commun*. 12:4578.

Flores-Rodriguez, N., S. Rogers, D. Kenwright, T. Waigh, P. Woodman, and V. Allan. 2011. Roles of dynein and dynactin in early endosome dynamics revealed using automated tracking and global analysis. *PLoS ONE*. 6:e24479.

Gama, J.B., C. Pereira, P.A. Simoes, R. Celestino, R.M. Reis, D.J. Barbosa, H.R. Pires, C. Carvalho, J. Amorim, A.X. Carvalho, D.K. Cheerambathur, and R. Gassmann. 2017. Molecular mechanism of dynein recruitment to kinetochores by the Rod-Zw10-Zwilch complex and Spindly. *J Cell Biol*. 216:943-960.

Gill, S.R., T.A. Schroer, I. Szilak, E.R. Steuer, and M.P. Sheetz. 1991. Dynactin, a conserved, ubiquitously expressed component of an activator of vesicle motility mediated by cytoplasmic dynein. *J. Cell Biol.* 115:1639-1650.

Gillies, J.P., J.M. Reimer, E.P. Karasmanis, I. Lahiri, Z.M. Htet, A.E. Leschziner, and S.L. Reck-Peterson. 2022. Structural Basis for Cytoplasmic Dynein-1 Regulation by Lis1. *eLife*. *In press*:In press.

Goncalves, J.C., T.J. Dantas, and R.B. Vallee. 2019. Distinct roles for dynein light intermediate chains in neurogenesis, migration, and terminal somal translocation. *J Cell Biol*. 218:808-819.

Gönczy, P., S. Pichler, M. Kirkham, and A. Hyman. 1999. Cytoplasmic dynein is required for distinct aspects of MTOC positioning, including centrosome separation, in the one cell stage *Caenorhabditis elegans* embryo. *J. Cell Biol.* 147:135-150.

Grabarek, Z. 2006. Structural basis for diversity of the EF-hand calcium-binding proteins. *J Mol Biol*. 359:509-525.

Granger, E., G. McNee, V. Allan, and P. Woodman. 2014. The role of the cytoskeleton and molecular motors in endosomal dynamics. *Semin Cell Dev Biol*. 31:20-29.

Grotjahn, D.A., S. Chowdhury, Y. Xu, R.J. McKenney, T.A. Schroer, and G.C. Lander. 2018. Cryo-electron tomography reveals that dynactin recruits a team of dyneins for processive motility. *Nat Struct Mol Biol*. 25:203-207.

Guo, X., G.G. Farias, R. Mattera, and J.S. Bonifacino. 2016. Rab5 and its effector FHF contribute to neuronal polarity through dynein-dependent retrieval of somatodendritic proteins from the axon. *Proc Natl Acad Sci U S A*. 113:E5318-5327.

Gutierrez, P.A., B.E. Ackermann, M. Vershinin, and R.J. McKenney. 2017. Differential effects of the dynein-regulatory factor Lissencephaly-1 on processive dynein-dynactin motility. *J Biol Chem*. 292:12245-12255.

Hamer, G., H. Wang, E. Bolcun-Filas, H.J. Cooke, R. Benavente, and C. Hoog. 2008. Progression of meiotic recombination requires structural maturation of the central element of the synaptonemal complex. *J Cell Sci*. 121:2445-2451.

1324 Hirotsune, S., M. Fleck, M. Gambello, G. Bix, A. Chen, G. Clark, D. Ledbetter, C. McBain, and
1325 A. Wynshaw-Boris. 1998. Graded reduction of Pafah1b1 (Lis1) activity results in
1326 neuronal migration deffects and early embryonic lethality. *Nat. Genet.* 19:333-339.
1327 Hoogenraad, C., A. Akhmanova, S. Howell, B. Dortland, C. de Zeeuw, R. Willemsen, P. Visser,
1328 F. Grosveld, and N. Galjart. 2001. Mammalian Golgi-associated Bicaudal-D2 functions
1329 in the dynein-dynactin pathway by interacting with these complexes. *EMBO J.*
1330 20:4041-4054.
1331 Hoogenraad, C., P. Wulf, N. Schiefermeier, T. Stepanova, N. Galjart, J. Small, F. Grosveld, C. de
1332 Zeeuw, and A. Akhmanova. 2003. Bicaudal D induces selective dynein-mediated
1333 microtubule minus end-directed transport. *EMBO J.* 22:6004-6015.
1334 Horgan, C.P., S.R. Hanscom, R.S. Jolly, C.E. Futter, and M.W. McCaffrey. 2010a. Rab11-FIP3
1335 binds dynein light intermediate chain 2 and its overexpression fragments the Golgi
1336 complex. *Biochemical and biophysical research communications*. 394:387-392.
1337 Horgan, C.P., S.R. Hanscom, R.S. Jolly, C.E. Futter, and M.W. McCaffrey. 2010b. Rab11-FIP3
1338 links the Rab11 GTPase and cytoplasmic dynein to mediate transport to the
1339 endosomal-recycling compartment. *J Cell Sci*. 123:181-191.
1340 Horgan, C.P., S.R. Hanscom, and M.W. McCaffrey. 2011. Dynein LIC1 localises to the mitotic
1341 spindle and midbody and LIC2 localises to spindle poles during cell division. *Cell Biol.*
1342 *Int.* doi:10.1042/CBI20100284.
1343 Horn, H., D.I. Kim, G. Wright, E. Wong, C. Stewart, B. Burke, and K. Roux. 2013. A mammalian
1344 KASH domain protein coupling meiotic chromosomes to the cytoskeleton. *J. Cell Biol.*
1345 202:1023-1039.
1346 Htet, Z.M., J.P. Gillies, R.W. Baker, A.E. Leschziner, M.E. DeSantis, and S.L. Reck-Peterson.
1347 2020. LIS1 promotes the formation of activated cytoplasmic dynein-1 complexes. *Nat*
1348 *Cell Biol*. 22:518-525.
1349 Hunt, S., A. Townley, C. Danson, P.J. Cullen, and D.J. Stephens. 2013. Microtubule motors
1350 mediate endosomal sorting by maintaining functional domain organization. *J. Cell Sci.*
1351 126:2493-2501.
1352 Jha, R., J. Roostalu, N.I. Cade, M. Trokter, and T. Surrey. 2017. Combinatorial regulation of the
1353 balance between dynein microtubule end accumulation and initiation of directed
1354 motility. *EMBO J*. 36:3387-3404.

1355 Johansson, M., N. Rocha, W. Zwart, I. Jordens, L. Janssen, C. Kuijl, V. Olkkonen, and J. Neefjes.
1356 2007. Activation of endosomal dynein motors by stepwise assembly of Rab7-RILP-
1357 p150Glued, ORP1L and the receptor bIII spectrin. *J. Cell Biol.* 176:459-471.
1358 Jones, L., C. Villemant, T. Starborg, A. Salter, G. Goddard, P. Ruane, P. Woodman, N.
1359 Papalopulu, S. Woolner, and V. Allan. 2014. Dynein light intermediate chains maintain
1360 spindle bipolarity by functioning in centriole cohesion. *J. Cell Biol.* 207:499-516.
1361 Jordens, I., M. Fernandez-Borja, M. Marsman, S. Dusseljee, L. Janssen, J. Calafat, H. Janssen,
1362 R. Wubbolts, and J. Neefjes. 2001. The Rab7 effector protein RILP controls lysosomal
1363 transport by inducing the recruitment of dynein-dynactin motors. *Curr. Biol.* 11:1680-
1364 1685.
1365 Karki, S., and E.L.F. Holzbaur. 1995. Affinity chromatography demonstrates a direct binding
1366 between cytoplasmic dynein and the dynactin complex. *J. Biol. Chem.* 270:28806-
1367 28811.
1368 King, S., C. Brown, K. Maier, N. Quintyne, and T. Schroer. 2003. Analysis of the dynein-dynactin
1369 interaction in vitro and in vivo. *Mol. Biol. Cell*. 14:5089-5097.
1370 Koszul, R., K.P. Kim, M. Prentiss, N. Kleckner, and S. Kameoka. 2008. Meiotic chromosomes
1371 move by linkage to dynamic actin cables with transduction of force through the
1372 nuclear envelope. *Cell*. 133:1188-1201.
1373 Kumari, A., C. Kumar, R. Pergu, M. Kumar, S.P. Mahale, N. Wasnik, and S.V.S. Mylavarapu.
1374 2021a. Phosphorylation and Pin1 binding to the LIC1 subunit selectively regulate
1375 mitotic dynein functions. *J Cell Biol*. 220.
1376 Kumari, A., C. Kumar, N. Wasnik, and S.V.S. Mylavarapu. 2021b. Dynein light intermediate
1377 chains as pivotal determinants of dynein multifunctionality. *J Cell Sci*. 134.
1378 Lam, C., M.A. Vergnolle, L. Thorpe, P. Woodman, and V. Allan. 2010. Functional interplay
1379 between LIS1, NDE1 and NDEL1 in dynein-dependent organelle positioning. *J Cell Sci*.
1380 123:202-212.
1381 Lau, C.K., F.J. O'Reilly, B. Santhanam, S.E. Lacey, J. Rappsilber, and A.P. Carter. 2021. Cryo-EM
1382 reveals the complex architecture of dynactin's shoulder region and pointed end.
1383 *EMBO J*. 40:e106164.
1384 Lee, C.Y., H.F. Horn, C.L. Stewart, B. Burke, E. Bolcun-Filas, J.C. Schimenti, M.E. Dresser, and
1385 R.J. Pezza. 2015. Mechanism and regulation of rapid telomere prophase movements
1386 in mouse meiotic chromosomes. *Cell Rep*. 11:551-563.

1387 Lee, I.G., S.E. Cason, S.S. Alqassim, E.L.F. Holzbaur, and R. Dominguez. 2020. A tunable LIC1-
1388 adaptor interaction modulates dynein activity in a cargo-specific manner. *Nat*
1389 *Commun*. 11:5695.
1390 Lee, I.G., M.A. Olenick, M. Boczkowska, C. Franzini-Armstrong, E.L.F. Holzbaur, and R.
1391 Dominguez. 2018. A conserved interaction of the dynein light intermediate chain with
1392 dynein-dynactin effectors necessary for processivity. *Nat Commun*. 9:986.
1393 Lee, Y.L., and B. Burke. 2018. LINC complexes and nuclear positioning. *Semin Cell Dev Biol*.
1394 82:67-76.
1395 Lindeman, R.E., and F. Pelegri. 2012. Localized Products of futile cycle/ lrmp Promote
1396 Centrosome-Nucleus Attachment in the Zebrafish Zygote. *Current Biology*. 22:843-
1397 851.
1398 Link, J., M. Leubner, J. Schmitt, E. Gob, R. Benavente, K.T. Jeang, R. Xu, and M. Alsheimer.
1399 2014. Analysis of meiosis in SUN1 deficient mice reveals a distinct role of SUN2 in
1400 mammalian meiotic LINC complex formation and function. *PLoS Genet*. 10:e1004099.
1401 Liu, H., T. Huang, M. Li, M. Li, C. Zhang, J. Jiang, X. Yu, Y. Yin, F. Zhang, G. Lu, M.C. Luo, L.R.
1402 Zhang, J. Li, K. Liu, and Z.J. Chen. 2019. SCRE serves as a unique synaptonemal complex
1403 fastener and is essential for progression of meiosis prophase I in mice. *Nucleic Acids*
1404 *Res*. 47:5670-5683.
1405 Mahale, S., M. Kumar, A. Sharma, A. Babu, S. Ranjan, C. Sachidanandan, and S.V.S.
1406 Mylavarapu. 2016a. The Light Intermediate Chain 2 Subpopulation of Dynein
1407 Regulates Mitotic Spindle Orientation. *Sci Rep*. 6:22.
1408 Mahale, S.P., A. Sharma, and S.V. Mylavarapu. 2016b. Dynein Light Intermediate Chain 2
1409 Facilitates the Metaphase to Anaphase Transition by Inactivating the Spindle
1410 Assembly Checkpoint. *PLoS One*. 11:e0159646.
1411 Malone, C., L. Misner, N. Le Bot, M.-C. Tsai, J. Campbell, J. Ahringher, and J. White. 2003. The
1412 *C. elegans* hook protein, ZYG12, mediates the essential attachment between the
1413 centrosome and nucleus. *Cell*. 115:825-836.
1414 Markus, S.M., M.G. Marzo, and R.J. McKenney. 2020. New insights into the mechanism of
1415 dynein motor regulation by lissencephaly-1. *Elife*. 9.
1416 Marzo, M.G., J.M. Griswold, and S.M. Markus. 2020. Pac1/LIS1 stabilizes an uninhibited
1417 conformation of dynein to coordinate its localization and activity. *Nat Cell Biol*. 22:559-
1418 569.

McKenney, R., H. W, M. Tanenbaum, G. Bhabha, and R.D. Vale. 2014. Activation of cytoplasmic dynein motility by dynactin-cargo adatper complexes. *Science*. 345:337-341.

Minn, I.L., M.M. Rolls, W. Hanna-Rose, and C.J. Malone. 2009. SUN-1 and ZYG-12, Mediators of Centrosome–Nucleus Attachment, Are a Functional SUN/KASH Pair in. *Molecular biology of the cell*. 20:4586-4595.

Morimoto, A., H. Shibuya, X. Zhu, J. Kim, K.i. Ishiguro, M. Han, and Y. Watanabe. 2012. A conserved KASH domain protein associates with telomeres, SUN1, and dynactin during mammalian meiosis. *J. Cell Biol.* 198:165-172.

Niclas, J., V.J. Allan, and R.D. Vale. 1996. Cell cycle regulation of dynein association with membranes modulates microtubule-based organelle transport. *J. Cell Biol.* 133:585-593.

Olenick, M.A., R. Dominguez, and E.L.F. Holzbaur. 2019. Dynein activator Hook1 is required for trafficking of BDNF-signaling endosomes in neurons. *J Cell Biol*. 218:220-233.

Olenick, M.A., and E.L.F. Holzbaur. 2019. Dynein activators and adaptors at a glance. *J Cell Sci*. 132.

Olsen, J.V., M. Vermeulen, A. Santamaria, C. Kumar, M.L. Miller, L.J. Jensen, F. Gnad, J. Cox, T.S. Jensen, E.A. Nigg, S. Brunak, and M. Mann. 2010. Quantitative phosphoproteomics reveals widespread full phosphorylation site occupancy during mitosis. *Sci Signal*. 3:ra3.

Palmer, K.J., H. Hughes, and D.J. Stephens. 2009. Specificity of Cytoplasmic Dynein Subunits in Discrete Membrane Trafficking Steps. *Mol Biol Cell*. 20:2885-2899.

Pandey, J., and D. Smith. 2011. A Cdk5-dependent switch regulates Lis1/Ndel1/dynein-driven organelle transport in adult neurons. *J. Neurosci.* 31:17207-17219.

Payne, C., V. Rawe, J. Ramalho-Santos, C. Simerly, and G. Schatten. 2003. Preferentially localized dynein and perinuclear dynactin associate with nuclear pore complex proteins to mediate genomic union during mammalian fertlization. *J. Cell Sci.* 116:4727-4738.

Peranen, J., M. Rikkonen, M. Hyvonen, and L. Kaariainen. 1996. T7 vectors with modified T7lac promoter for expression of proteins in Escherichia coli. *Anal Biochem*. 236:371-373.

1449 Pfister, K., E. Fisher, I. GIbbons, T. Hays, E. Holzbaur, J. McIntosh, M. Porter, T. Schroer, K.
1450 Vaughan, G. Witman, S. King, and R. Vallee. 2005. Cytoplasmic dynein nomenclature.
1451 *J. Cell Biol.* 171:411-413.
1452 Qiu, R., J. Zhang, and X. Xiang. 2019. LIS1 regulates cargo-adapter-mediated activation of
1453 dynein by overcoming its autoinhibition in vivo. *J Cell Biol*. 218:3630-3646.
1454 Quintyne, N., S. Gill, D. Eckley, C. Crego, D. Compton, and T. Schroer. 1999. Dynactin is
1455 required for microtubule anchoring at centrosomes. *J. Cell Biol.* 147:321-334.
1456 Raaijmakers, J., M. Tannenbaum, and R. Medema. 2013. Systematic dissection of dynein
1457 regulators in mitosis. *J. Cell Biol.* 201:201-215.
1458 Reck-Peterson, S.L., W.B. Redwine, R.D. Vale, and A.P. Carter. 2018. The cytoplasmic dynein
1459 transport machinery and its many cargoes. *Nat Rev Mol Cell Biol*. 19:382-398.
1460 Reddy, B.J., M. Mattson, C.L. Wynne, O. Vadpey, A. Durra, D. Chapman, R.B. Vallee, and S.P.
1461 Gross. 2016. Load-induced enhancement of Dynein force production by LIS1-NudE in
1462 vivo and in vitro. *Nat Commun*. 7:12259.
1463 Redwine, W.B., M.E. DeSantis, I. Hollyer, Z.M. Htet, P.T. Tran, S.K. Swanson, L. Florens, M.P.
1464 Washburn, and S.L. Reck-Peterson. 2017. The human cytoplasmic dynein interactome
1465 reveals novel activators of motility. *Elife*. 6.
1466 Reiner, O., R. Carrozzo, Y. Shen, M. Wehnert, F. Faustinella, W. Dobyns, T. Caskey, and D.
1467 Ledbetter. 1993. Isolation of a Miller-Dieker lissencephaly gene containing a G protein
1468 b-subunit-like repeat. *Nature*. 364:717-721.
1469 Reinsch, S., and E. Karsenti. 1997. Movement of nuclei along microtubules in *Xenopus* egg
1470 extracts. *Curr. Biol.* 7:211-214.
1471 Robinson, J., E. Wojcik, M. Sanders, M. McGrail, and T.S. Hays. 1999. Cytoplasmic dynein is
1472 required for the nuclear attachment and migration of centrosomes duing mitosis in
1473 *Drosophila. J Cell Biol*. 146:597-608.
1474 Rog, O., and A. Dernburg. 2015. Direct Visualization Reveals Kinetics of Meiotic Chromosome
1475 Synapsis. *Cell Rep.* 10:1639-1645.
1476 Sato, A., B. Isaac, C.M. Phillips, R. Rillo, P.M. Carlton, D.J. Wynne, R.A. Kasad, and A.F.
1477 Dernburg. 2009. Cytoskeletal Forces Span the Nuclear Envelope to Coordinate Meiotic
1478 Chromosome Pairing and Synapsis. *Cell*. 139:907-919.
1479 Scherer, J., J. Yi, and R. Vallee. 2014. PKA-dependent dynein switching from lysosomes to
1480 adenovirus: a novel form of host-virus competition. *J Cell Biol*. 205:163-177.

1481 Schlager, M.A., H. Hoang, L. Urnavicius, S. Bullock, and A.P. Carter. 2014a. In vitro
1482 reconstitution of a highly processive recombinant human dynein complex. *Embo J*.
1483 33:1855-1868.
1484 Schlager, M.A., A. Serra-Marques, I. Grigoriev, L.F. Gumy, M. Esteves da Silva, P.S. Wulf, A.
1485 Akhmanova, and C.C. Hoogenraad. 2014b. Bicaudal d family adaptor proteins control
1486 the velocity of Dynein-based movements. *Cell Rep*. 8:1248-1256.
1487 Schmitt, J., R. Benavente, D. Hodzic, C. Hoog, C.L. Stewart, and M. Alsheimer. 2007.
1488 Transmembrane protein Sun2 is involved in tethering mammalian meiotic telomeres
1489 to the nuclear envelope. *Proc Natl Acad Sci U S A*. 104:7426-7431.
1490 Schmoranzer, J., J.P. Fawcett, M. Segura, S. Tan, R.B. Vallee, T. Pawson, and G.G. Gundersen.
1491 2009. Par3 and Dynein Associate to Regulate Local Microtubule Dynamics and
1492 Centrosome Orientation during Migration. *Curr Biol*. 19:1065-1074.
1493 Schroeder, C., J. Olstrem, N. Hertz, and R. Vale. 2014. A Ras-like domain in the light
1494 intermediate chain bridges the dynein motor to a cargo-binding region. *eLife*.
1495 3:e03351-03322.
1496 Schroeder, C.M., and R.D. Vale. 2016. Assembly and activation of dynein–dynactin by the
1497 cargo adaptor protein Hook3. *J Cell Biol*. 214:309-318.
1498 Schroer, T.A., and M.P. Sheetz. 1991. Two activators of microtubule-based vesicle transport.
1499 *J. Cell Biol.* 115:1309-1318.
1500 Sharma, A., S. Dagar, and S.V.S. Mylavarapu. 2020. Transgelin-2 and phosphoregulation of the
1501 LIC2 subunit of dynein govern mitotic spindle orientation. *J Cell Sci*. 133.
1502 Shibuya, H., K. Ishiguro, and Y. Watanabe. 2014. The TRF1-binding protein TERB1 promotes
1503 chromosome movement and telomere rigidity in meiosis. *Nat Cell Biol*. 16:145-156.
1504 Siller, K.H., M. Serr, R. Steward, T.S. Hays, and C.Q. Doe. 2005. Live imaging of Drosophila brain
1505 neuroblasts reveals a role for Lis1/dynactin in spindle assembly and mitotic checkpoint
1506 control. *Mol Biol Cell*. 16:5127-5140.
1507 Sitaram, P., M. Anderson, J. Jodoin, E. Lee, and L. Lee. 2012. Regulation of dynein localization
1508 and centrosome positioning by Lis-1 and asunder during Drosophila spermatogenesis.
1509 *Development*. 39:2945-2954.
1510 Sivaram, M.V., T.L. Wadzinski, S.D. Redick, T. Manna, and S.J. Doxsey. 2009. Dynein light
1511 intermediate chain 1 is required for progress through the spindle assembly
1512 checkpoint. *Embo J*. 28:902-914.

1513 Sladewski, T.E., N. Billington, M.Y. Ali, C.S. Bookwalter, H. Lu, E.B. Krementsova, T.A. Schroer,
1514 and K.M. Trybus. 2018. Recruitment of two dyneins to an mRNA-dependent Bicaudal
1515 D transport complex. *Elife*. 7.
1516 Spindler, M.C., J. Redolfi, F. Helmprobst, P. Kollmannsberger, C. Stigloher, and R. Benavente.
1517 2019. Electron tomography of mouse LINC complexes at meiotic telomere attachment
1518 sites with and without microtubules. *Commun Biol*. 2:376.
1519 Splinter, D., D. Razafsky, M.A. Schlager, A. Serra-Marques, I. Grigoriev, J. Demmers, N. Keijzer,
1520 K. Jiang, I. Poser, A. Hyman, C.C. Hoogenraad, S. King, and A. Akhmanova. 2012. BICD2,
1521 dynactin and LIS1 cooperate in regulating dynein recruitment to cellular structures.
1522 *Mol. Biol. Cell*. 23:4226-4241.
1523 Srikanth, S., K.D. Kim, Y. Gao, J.S. Woo, S. Ghosh, G. Calmettes, A. Paz, J. Abramson, M. Jiang,
1524 and Y. Gwack. 2016. A large Rab GTPase encoded by CRACR2A is a component of
1525 subsynaptic vesicles that transmit T cell activation signals. *Sci Signal*. 9:ra31.
1526 Starr, D.A. 2011. KASH and SUN proteins. *Curr Biol*. 21:R414-415.
1527 Starr, D.A., and M. Han. 2002. Role of ANC-1 in tethering nuclei to the actin cytoskeleton.
1528 *Science*. 298:406-409.
1529 Tan, S., J. Scherer, and R. Vallee. 2011. Recruitment of dynein to late endosomes and
1530 lysosomes through light intermediate chains. *Mol Biol Cell*. 22:467-477.
1531 Torisawa, T., M. Ichikawa, A. Furuta, K. Saito, K. Oiwa, H. Kojima, Y.Y. Toyoshima, and K.a.y.
1532 Furuta. 2014. Autoinhibition and cooperative activation mechanisms of cytoplasmic
1533 dynein. *Nature cell biology*. 16:1118-1124.
1534 Trelles-Sticken, E., C. Adelfalk, J. Loidl, and H. Scherthan. 2005. Meiotic telomere clustering
1535 requires actin for its formation and cohesin for its resolution. *J Cell Biol*. 170:213-223.
1536 Tsai, J.W., Y. Chen, A.R. Kriegstein, and R.B. Vallee. 2005. LIS1 RNA interference blocks neural
1537 stem cell division, morphogenesis, and motility at multiple stages. *J Cell Biol*. 170:935-
1538 945.
1539 Tynan, S.H., M.A. Gee, and R.B. Vallee. 2000a. Distinct but overlapping sites within the
1540 cytoplasmic dynein heavy chain for dimerization and for intermediate chain and light
1541 intermediate chain binding. *J Biol Chem*. 275:32769-32774.
1542 Tynan, S.H., A. Purohit, S.J. Doxsey, and R.B. Vallee. 2000b. Light intermediate chain 1 defines
1543 a functional subfraction of cytoplasmic dynein which binds to pericentrin. *J. Biol.*
1544 *Chem.* 275:32763-32768.

1545 Urnavicius, L., C.K. Lau, M.M. Elshenawy, E. Morales-Rios, C. Motz, A. Yildiz, and A.P. Carter.
1546 2018. Cryo-EM shows how dynactin recruits two dyneins for faster movement.
1547 *Nature*. 554:202-206.
1548 Urnavicius, L., K. Zhang, A.G. Diamant, C. Motz, M.A. Schlager, M. Yu, N.A. Patel, C.V.
1549 Robinson, and A.P. Carter. 2015. The structure of the dynactin complex and its
1550 interaction with dynein. *Science*. 347:2630-2630.
1551 Vaughan, K.T., and R.B. Vallee. 1995. Cytoplasmic dynein binds dynactin through a direct
1552 interaction between the intermediate chains and p150Glued. *J. Cell Biol.* 131:1507-
1553 1516.
1554 Villari, G., C. Enrico Bena, M. Del Giudice, N. Gioelli, C. Sandri, C. Camillo, A. Fiorio Pla, C. Bosia,
1555 and G. Serini. 2020. Distinct retrograde microtubule motor sets drive early and late
1556 endosome transport. *EMBO J*. 39:e103661.
1557 Wang, S., S.A. Ketcham, A. Schon, B. Goodman, Y. Wang, J. Yates, 3rd, E. Freire, T.A. Schroer,
1558 and Y. Zheng. 2013. Nudel/NudE and Lis1 promote dynein and dynactin interaction in
1559 the context of spindle morphogenesis. *Mol Biol Cell*. 24:3522-3533.
1560 Wang, Y., W. Huynh, T.D. Skokan, W. Lu, A. Weiss, and R.D. Vale. 2019. CRACR2a is a calcium-
1561 activated dynein adaptor protein that regulates endocytic traffic. *J Cell Biol*. 218:1619-
1562 1633.
1563 Wilson, G.M., A.B. Fielding, G.C. Simon, X. Yu, P.D. Andrews, R.S. Hames, A.M. Frey, A.A.
1564 Peden, G.W. Gould, and R. Prekeris. 2005. The FIP3-Rab11 protein complex regulates
1565 recycling endosome targeting to the cleavage furrow during late cytokinesis. *Mol Biol*
1566 *Cell*. 16:849-860.
1567 Wortzel, I., G. Maik-Rachline, S.S. Yadav, T. Hanoch, and R. Seger. 2021. Mitotic HOOK3
1568 phosphorylation by ERK1c drives microtubule-dependent Golgi destabilization and
1569 fragmentation. *iScience*. 24:102670.
1570 Wozniak, M., B. Bola, K. Brownhill, Y.-C. Yang, V. Levakova, and V. Allan. 2009. Role of kinesin-
1571 1 and cytoplasmic dynein in endoplasmic reticulum movement in VERO cells. . *J. Cell*
1572 *Sci.* 122:1979-1989.
1573 Wynne, D., O. Rog, P. Carlton, and A.F. Dernburg. 2012. Dynein-dependent processive
1574 chromsome motions promote homologous pairing in *C. elegans* meiosis. *J. Cell Biol.*
1575 196:47-64.

Yi, J., K. Ori-McKenney, R. McKenny, M. Vershinin, S. Gross, and R. Vallee. 2011. High-resolution imaging reveals indirect coordination of opposite motors and a role for LIS1 in high-load axonal transport. *J. Cell Bio.* 195:193-201.

Zhang, K., H.E. Foster, A. Rondelet, S.E. Lacey, N. Bahi-Buisson, A.W. Bird, and A.P. Carter. 2017. Cryo-EM Reveals How Human Cytoplasmic Dynein Is Auto-inhibited and Activated. *Cell*. 169:1303-1314 e1318.

Zhang, Q., S.Y. Ji, K. Busayavalasa, J. Shao, and C. Yu. 2019. Meiosis I progression in spermatogenesis requires a type of testis-specific 20S core proteasome. *Nat Commun*. 10:3387.

Zufferey, R., D. Nagy, R.J. Mandel, L. Naldini, and D. Trono. 1997. Multiply attenuated lentiviral vector achieves efficient gene delivery in vivo. *Nat Biotechnol*. 15:871-875.

Garner et al. Figure 1

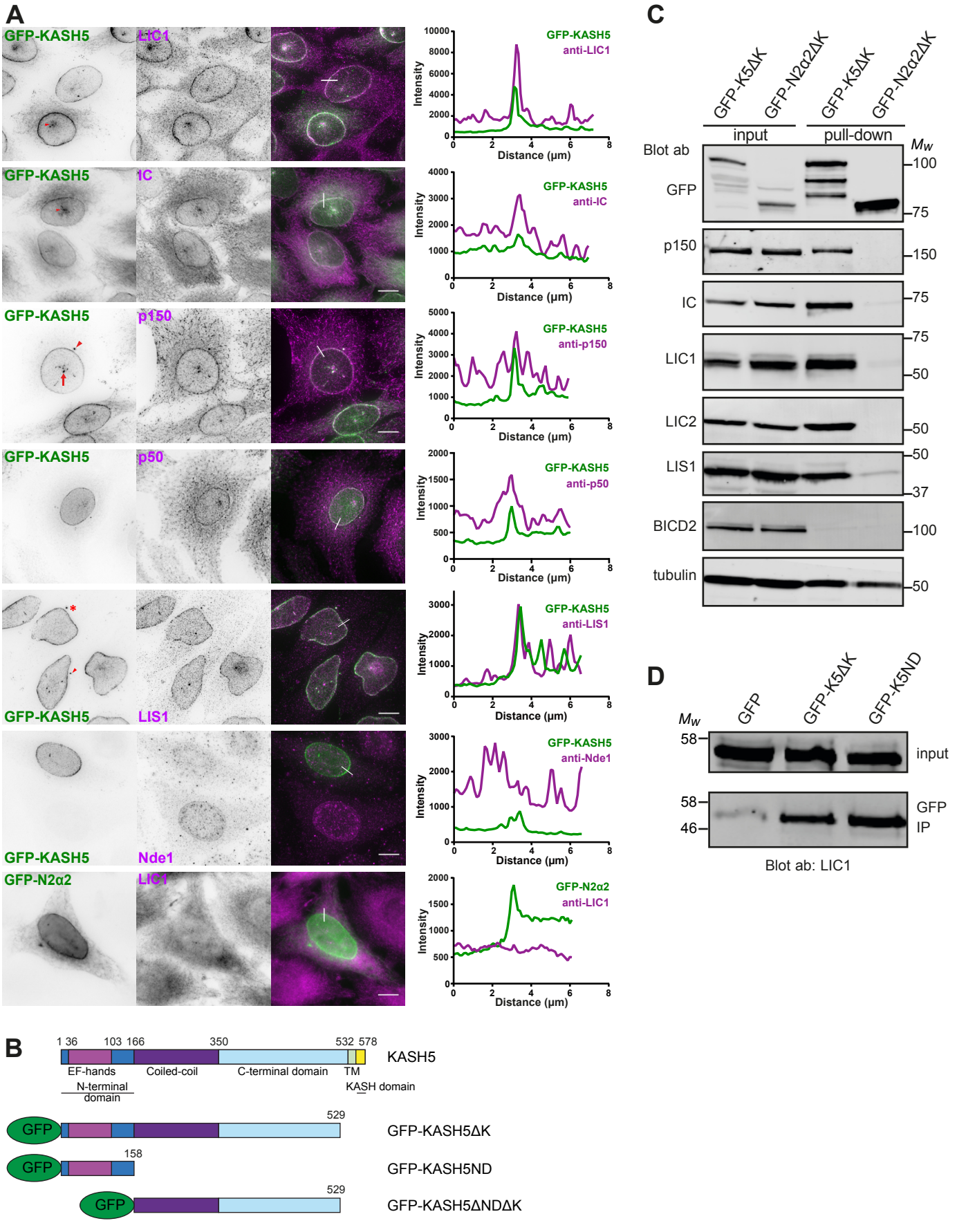

Garner et al. Figure 2

A IC2 siRNA

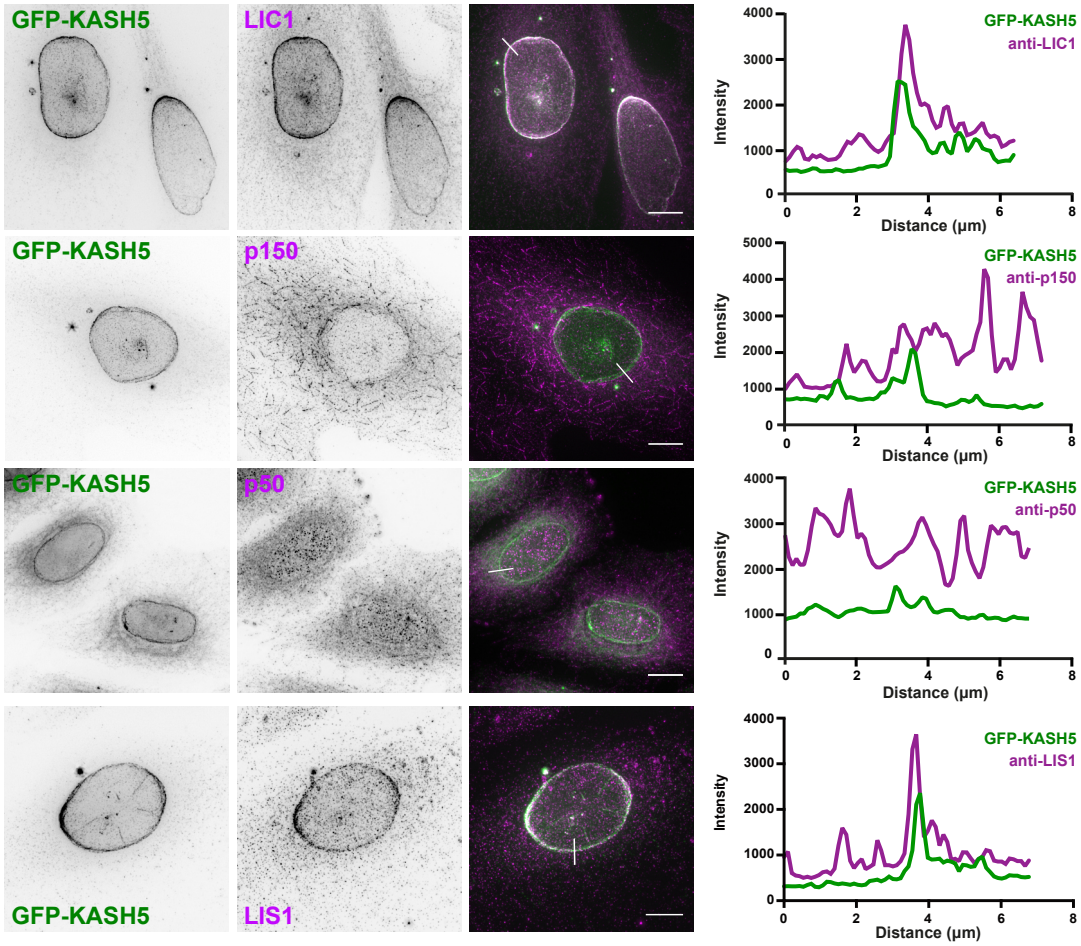

B RFP-p150-CC1 expression

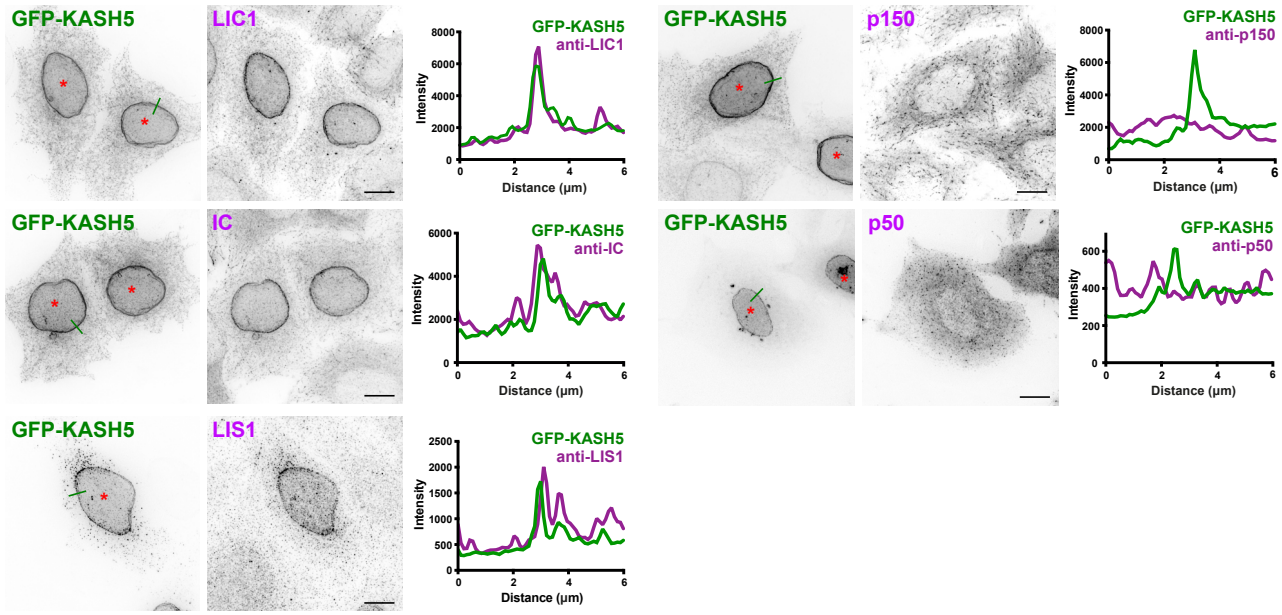

Garner et al. Figure 3

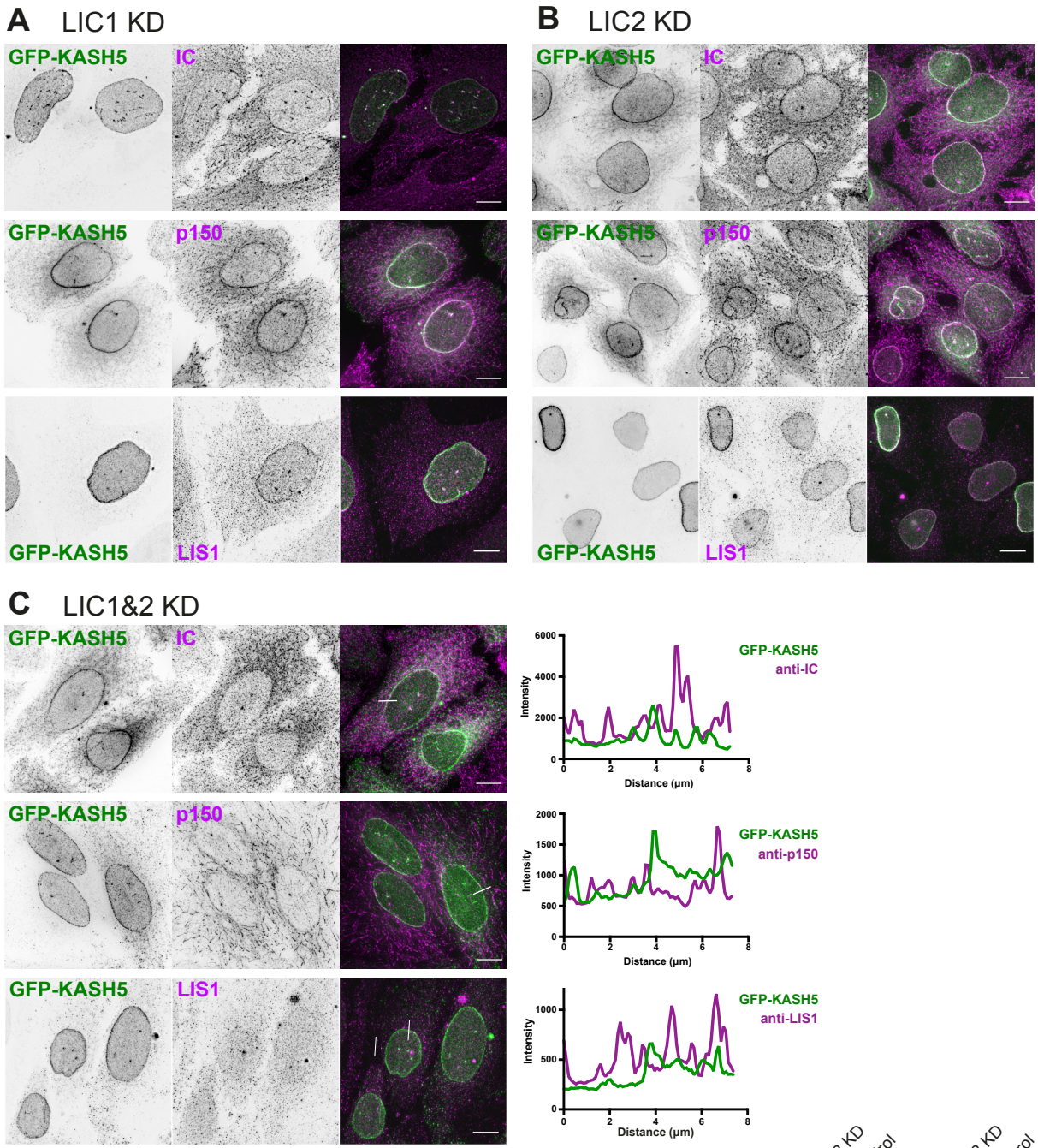

Figure 4, Garner et al.

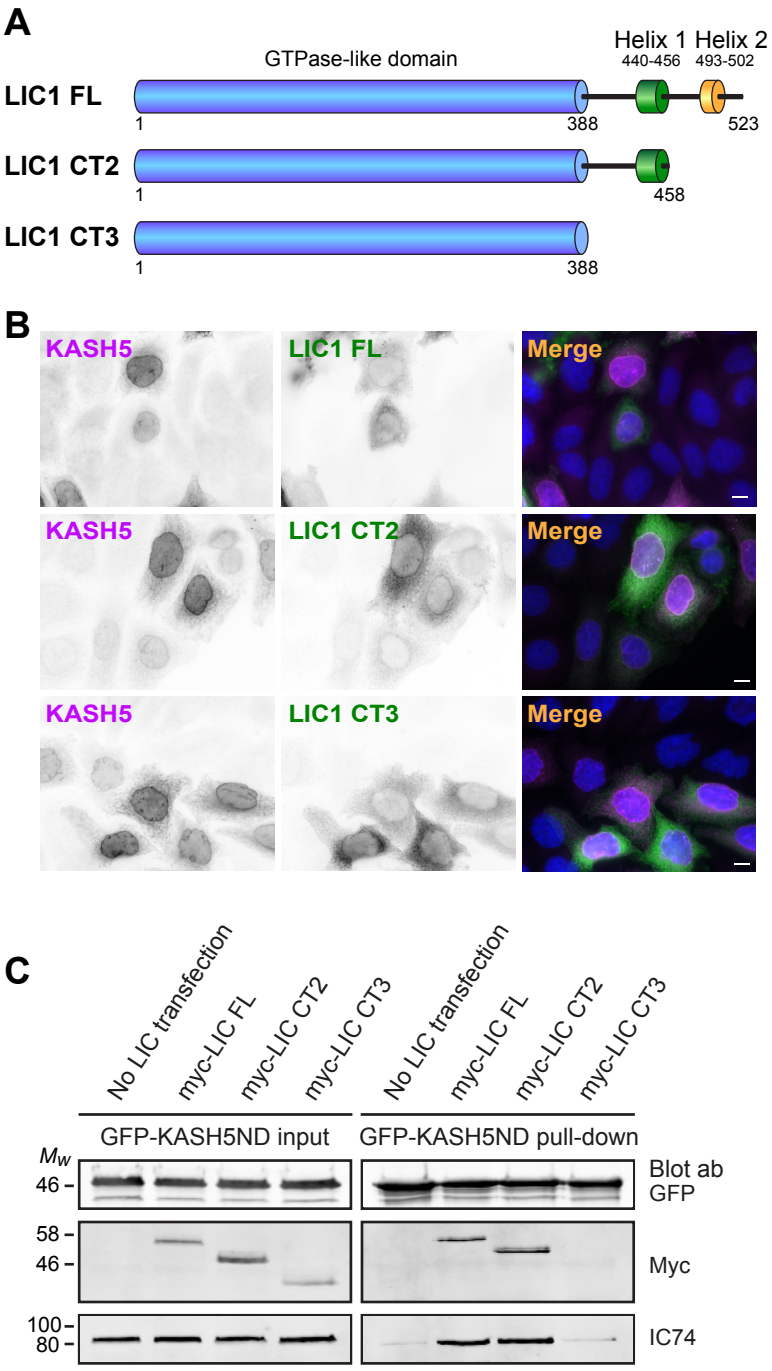

Figure 5, Garner et al.

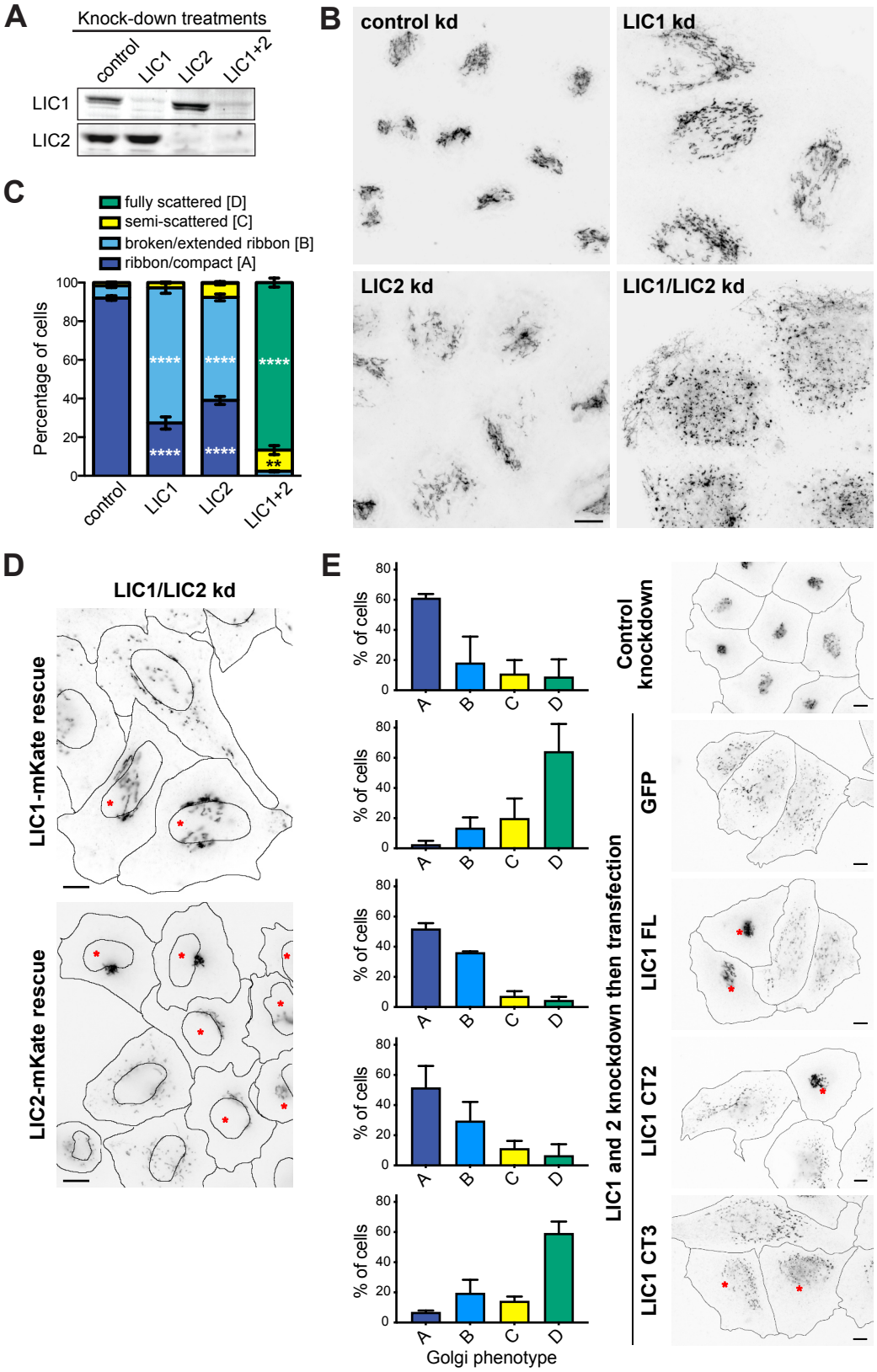

Figure 6, Garner et al.

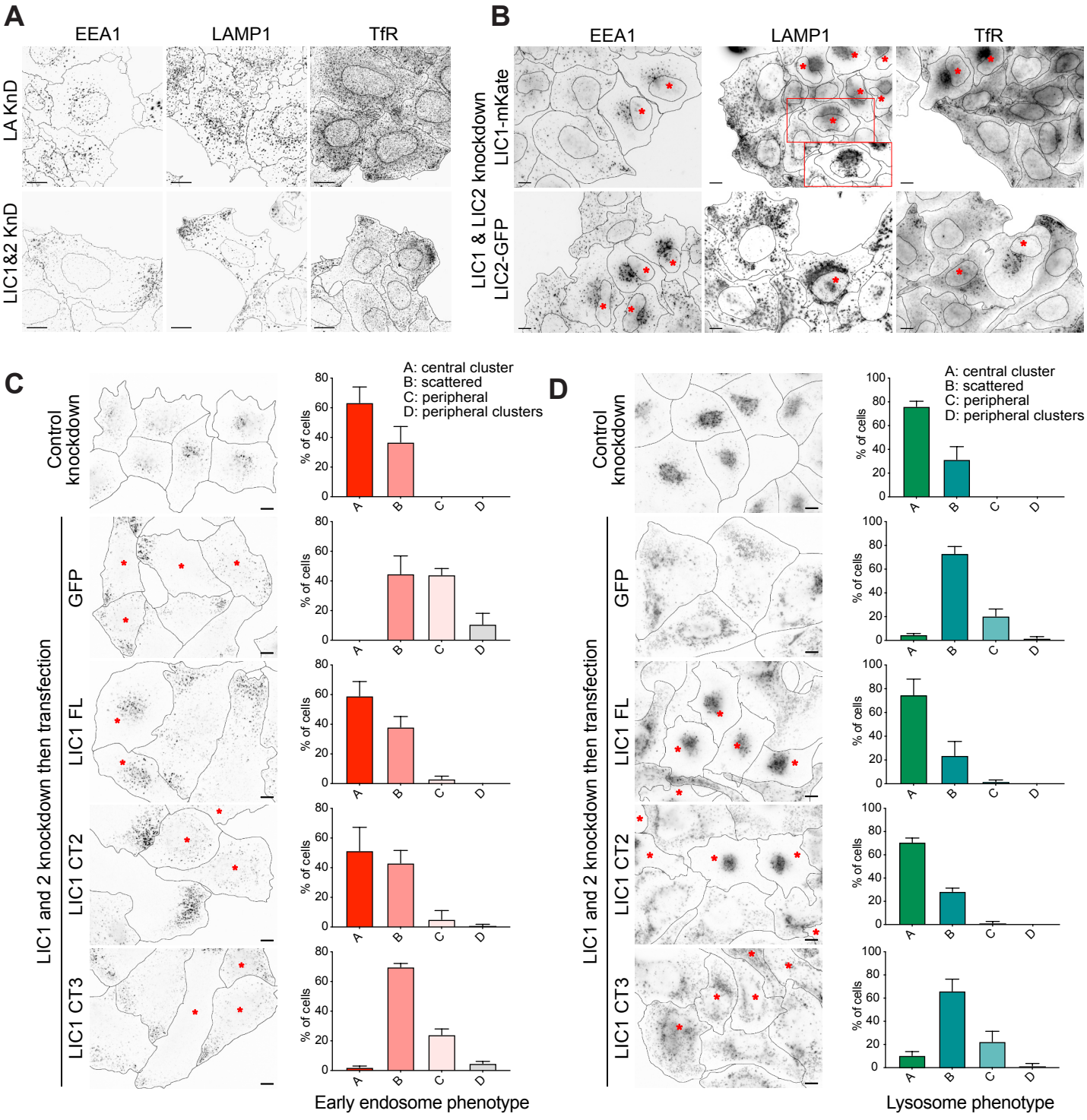

Figure 7, Garner et al.

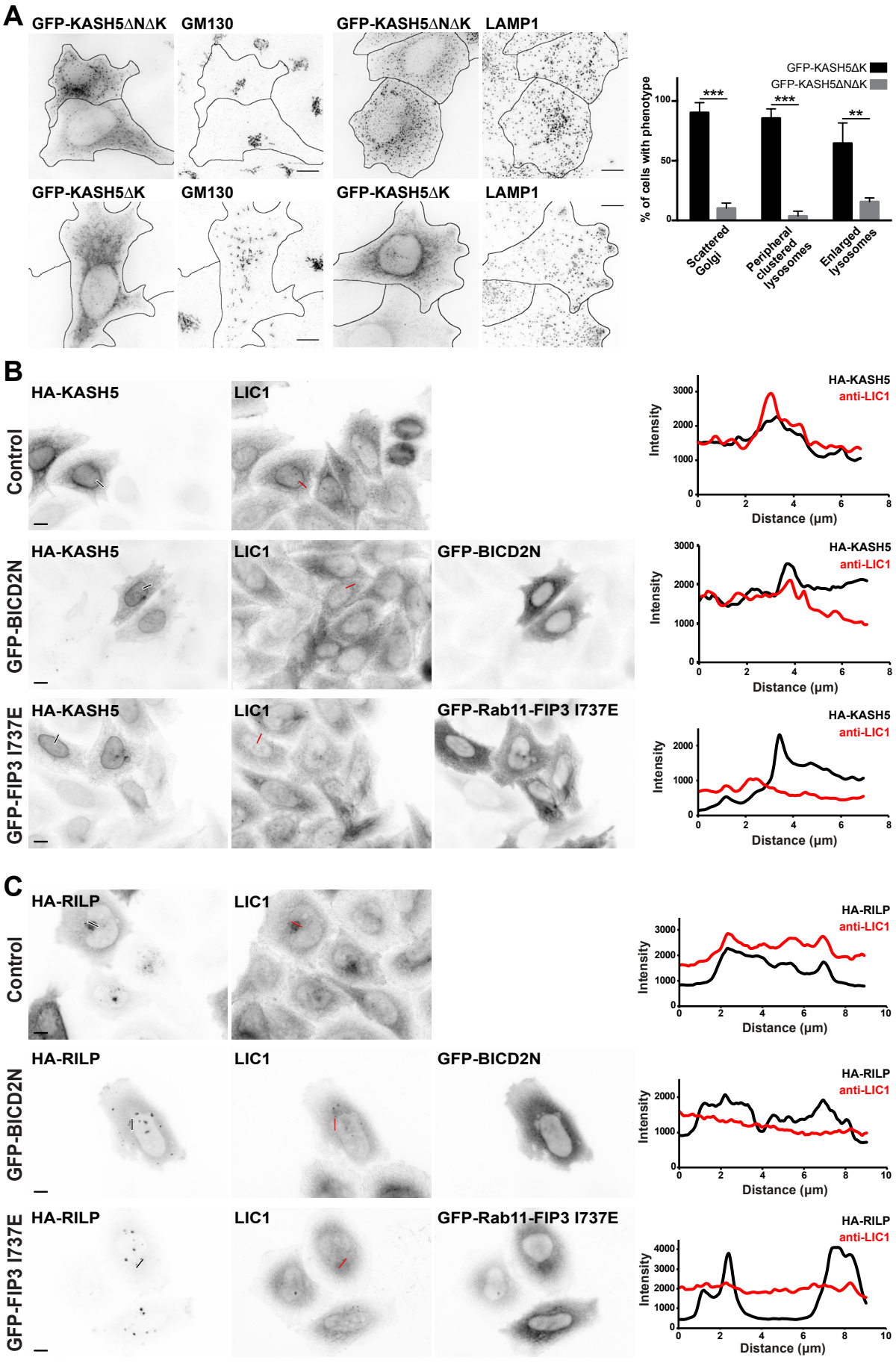

Garner et al. Figure 8

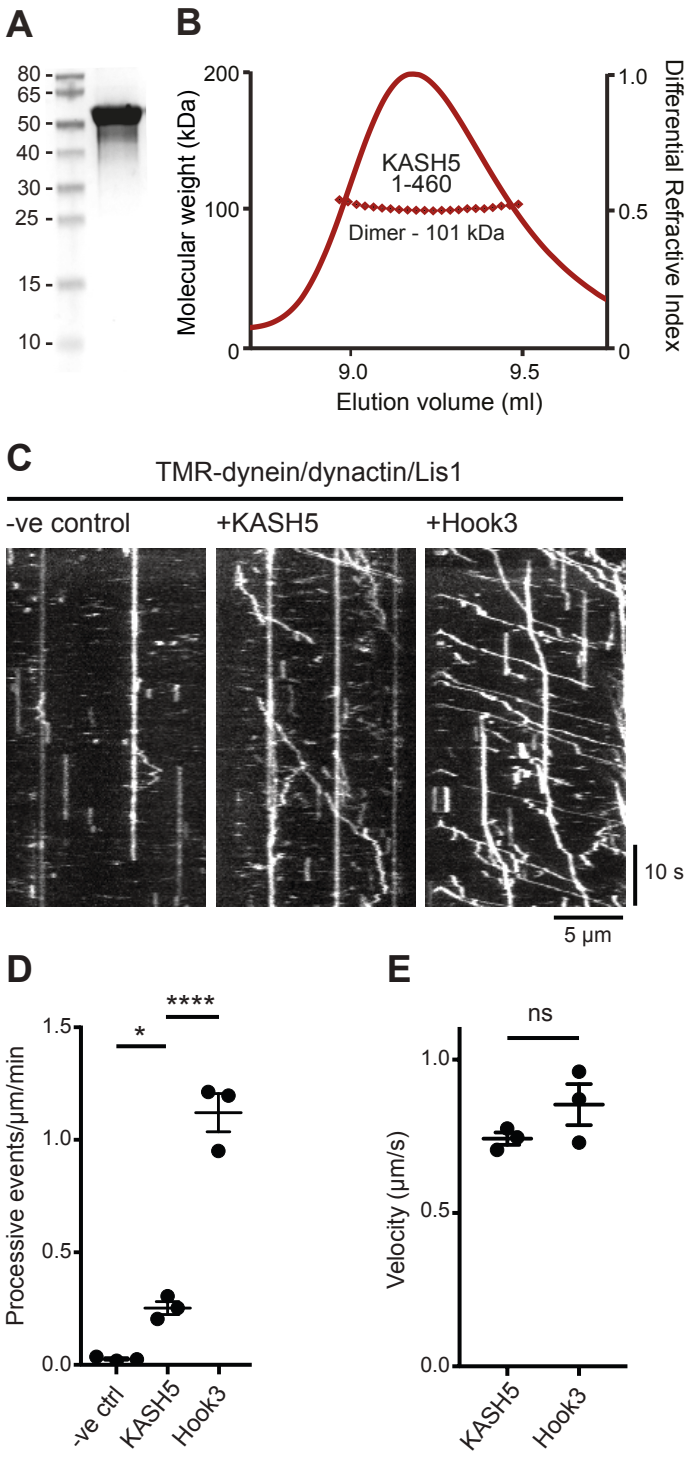

Figure 9, Garner et al.

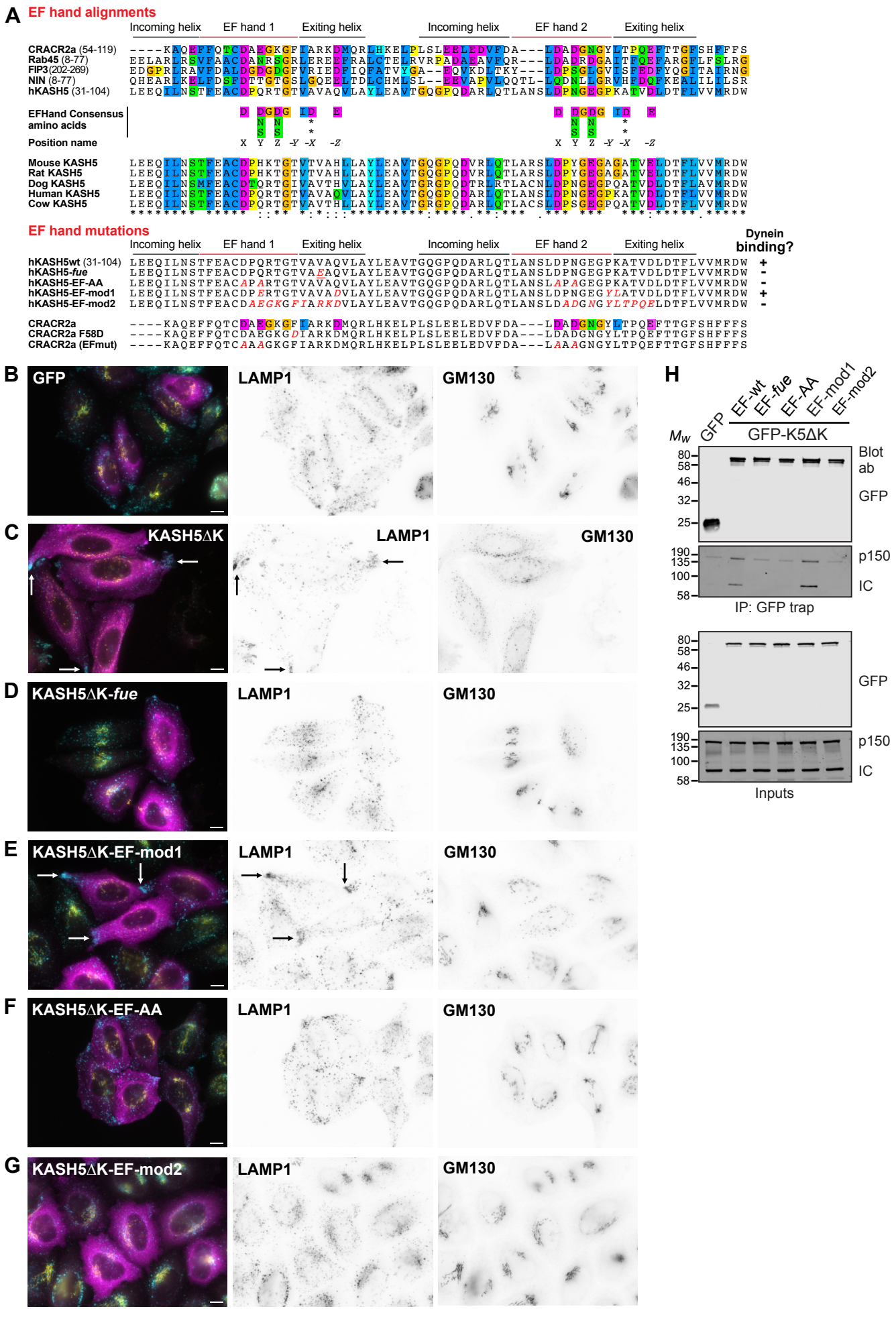

Garner et al., Supplementary Figure 1

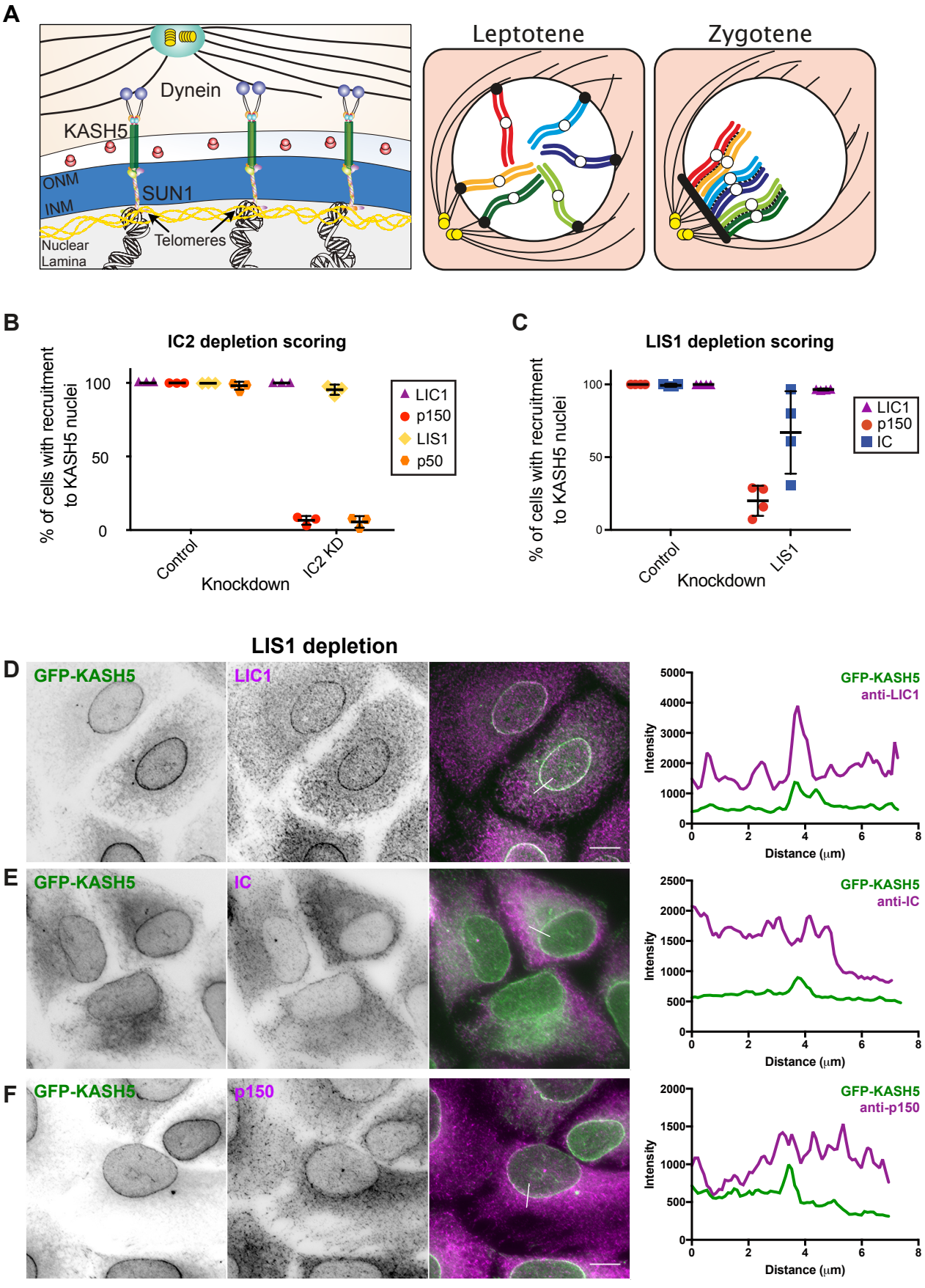

Garner et al. Supplementary Figure 2

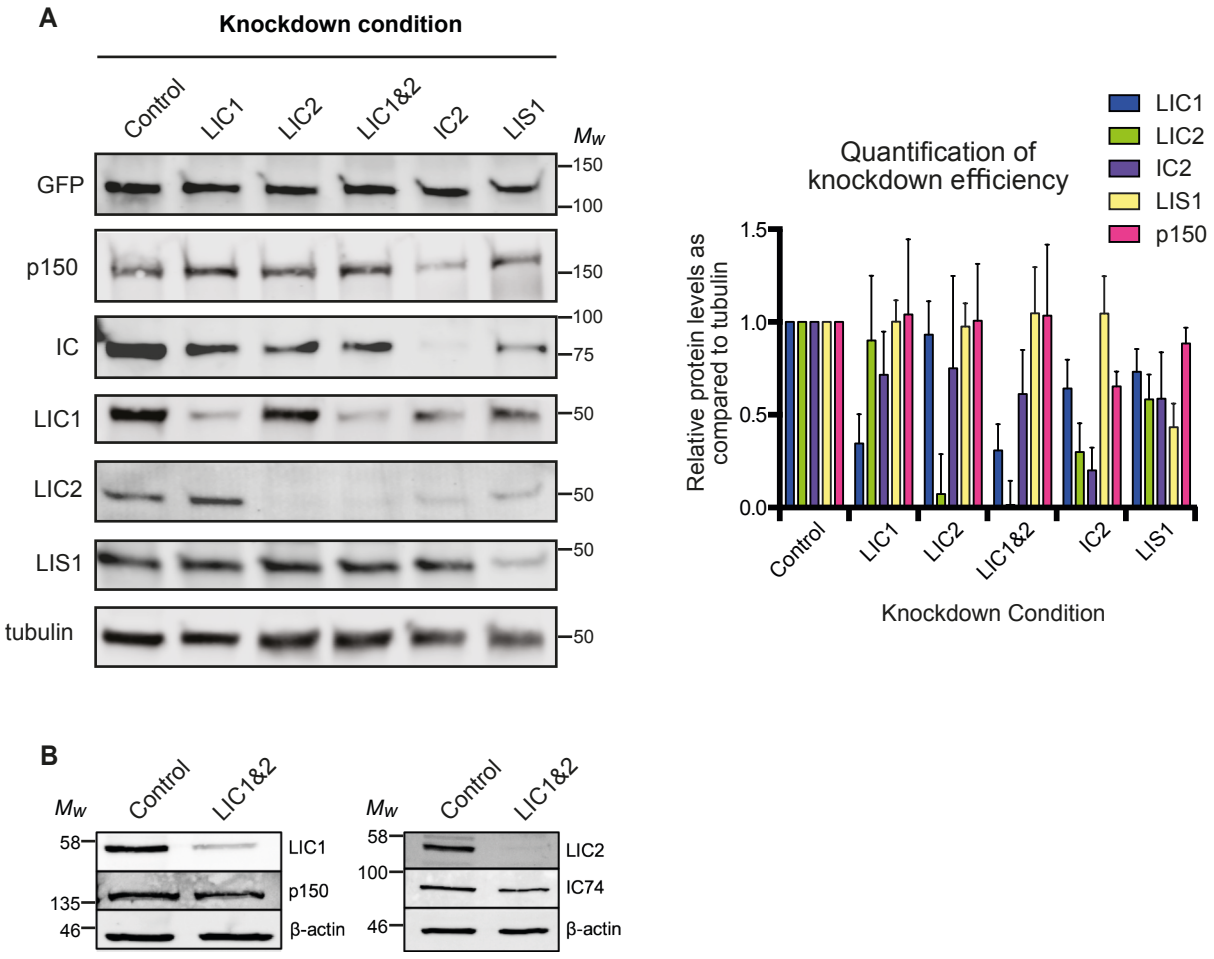

Garner et al. Supplementary Figure 3

Golgi apparatus phenotype scoring

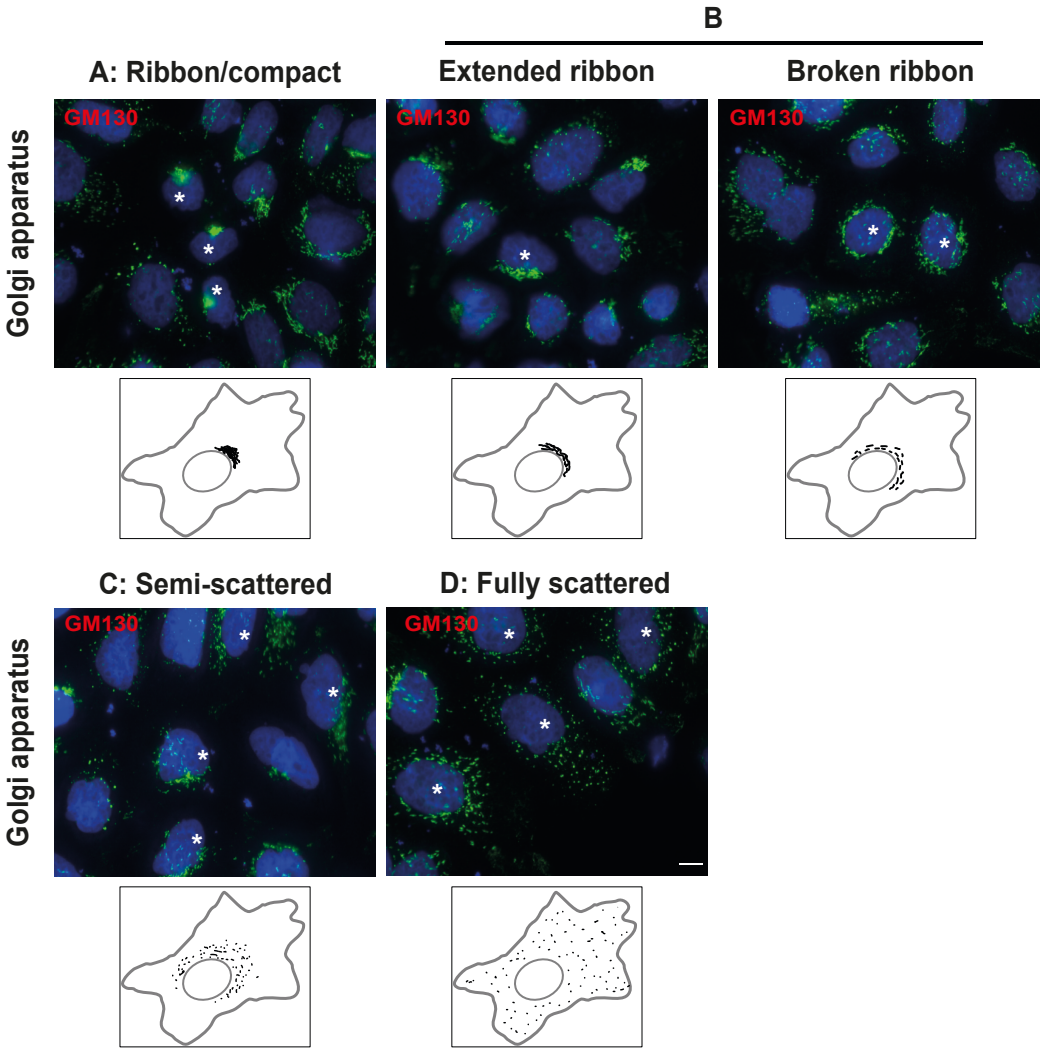

Early endosome and lysosome phenotype scoring

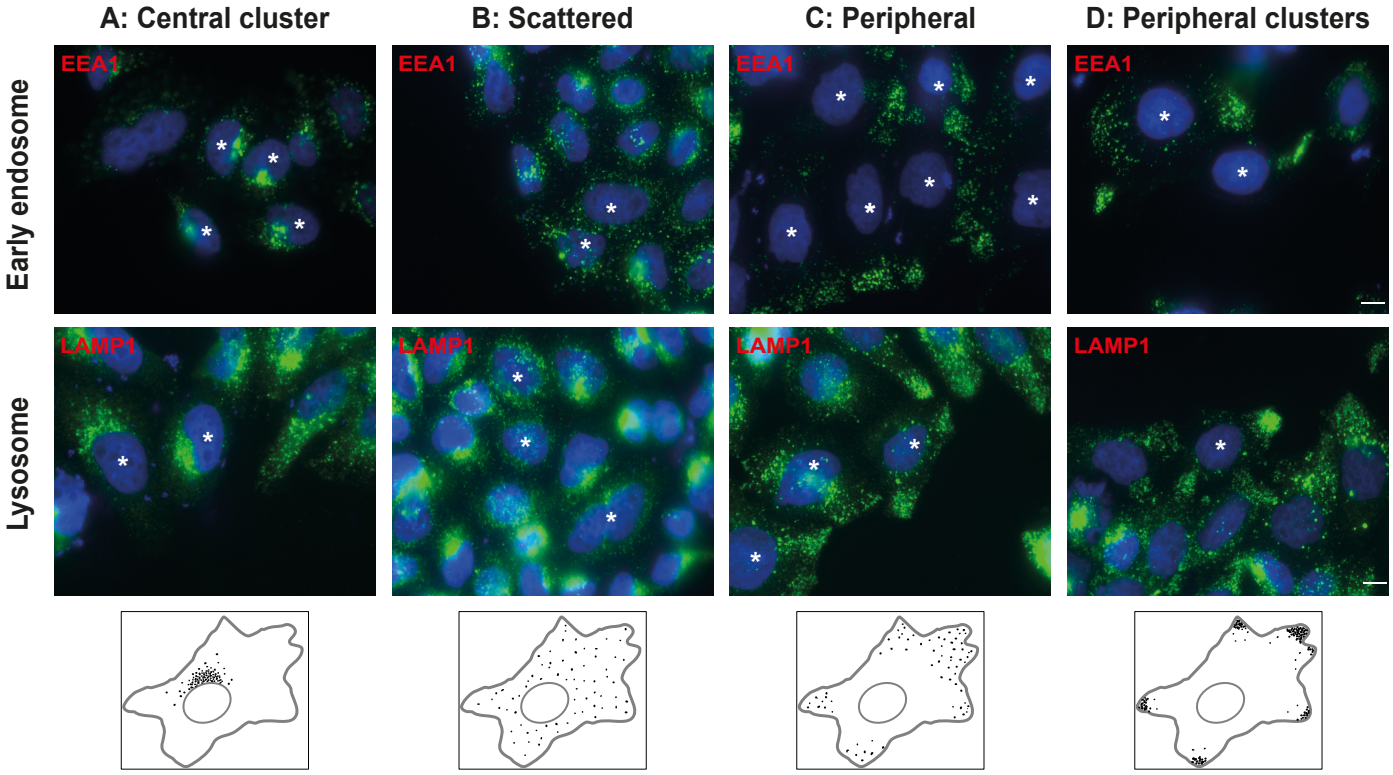

Garner et al. Supplementary Figure 4

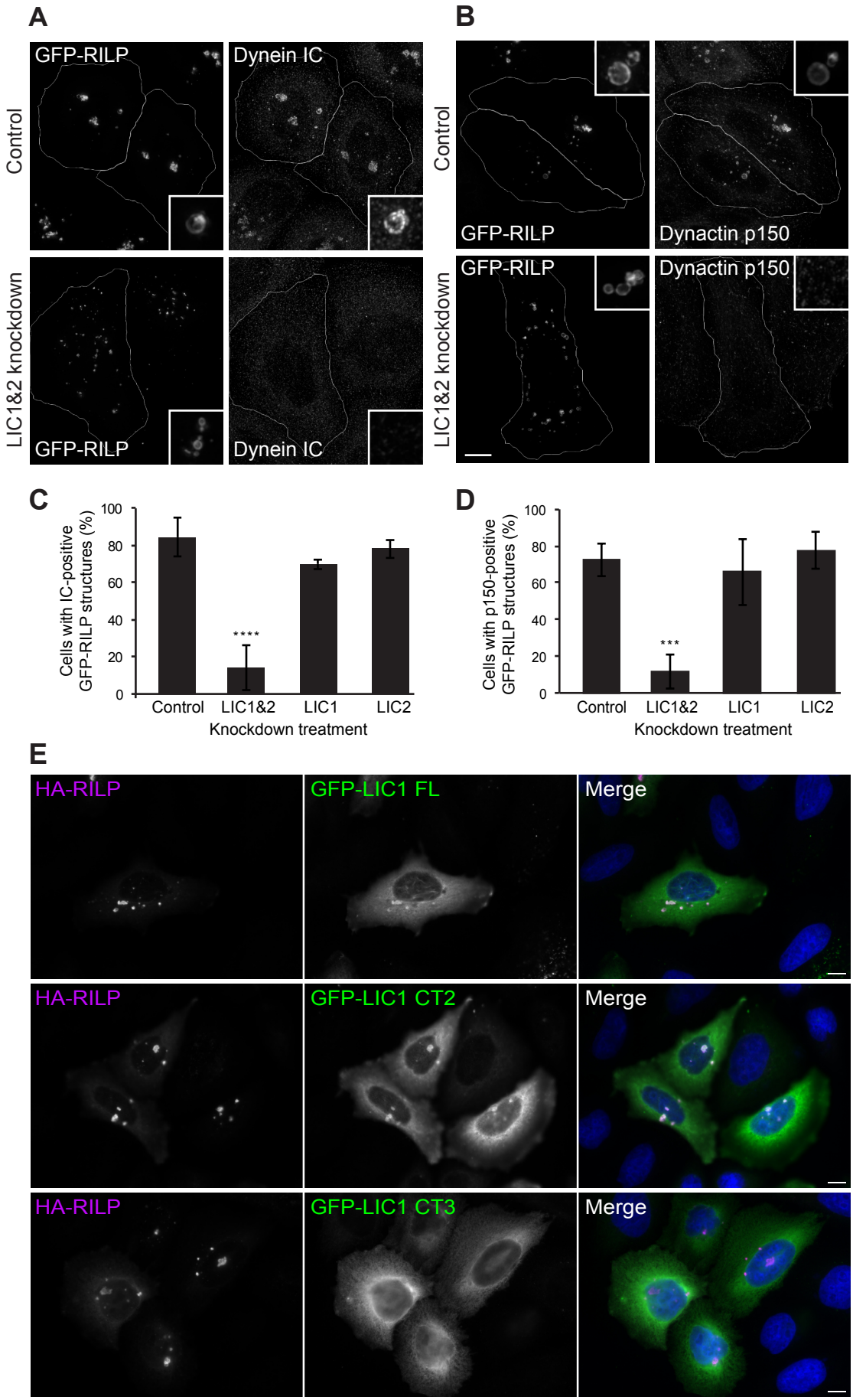

Garner et al. Supplementary Figure 5

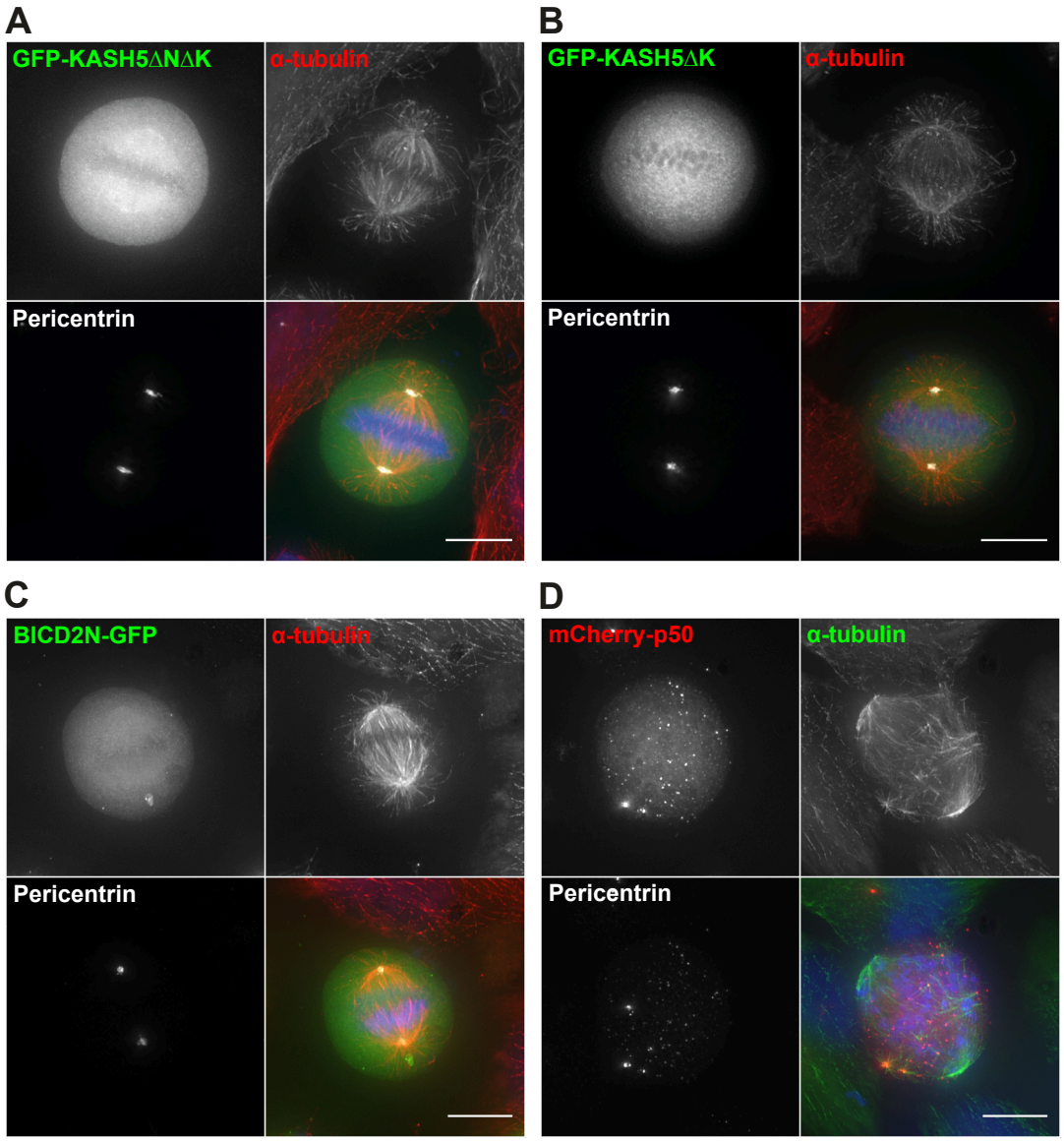

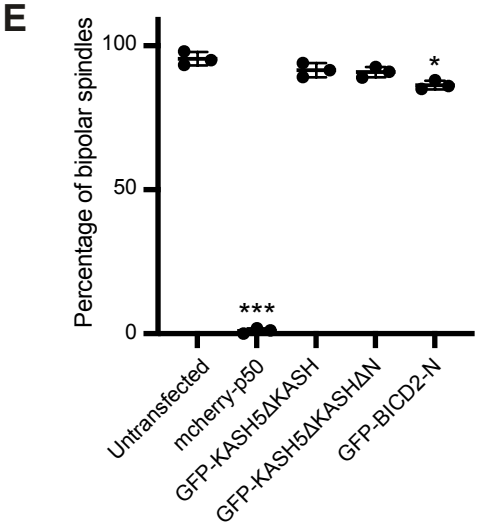

Garner et al. Supplementary Figure 6

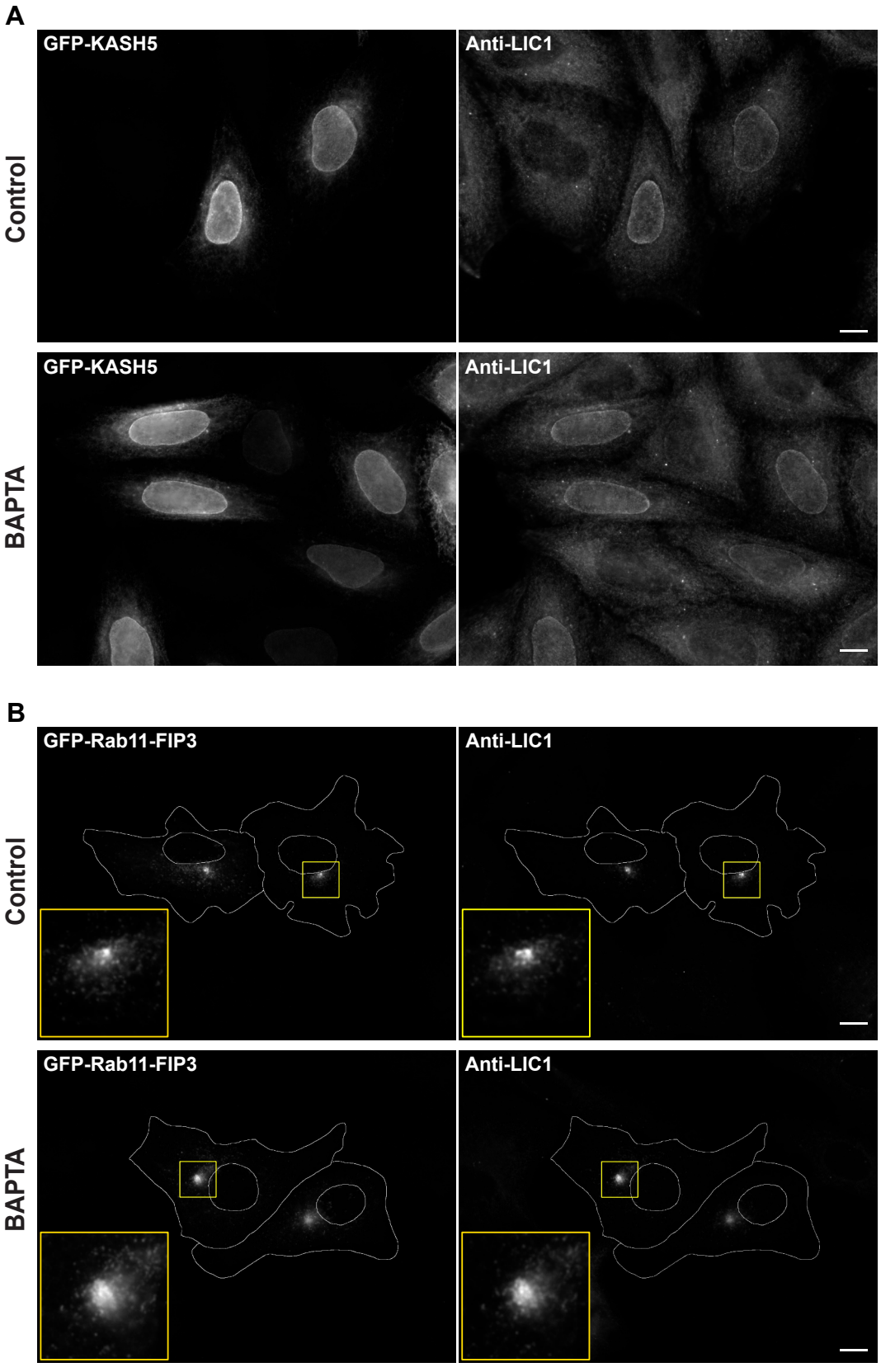

Table S1. Statistical analysis of the effects of LIC1 and LIC2 depletion on Golgi apparatus morphology.

The data presented graphically in Figure 5C were analysed by Two-way ANOVA with Tukey's test. P values are shown. Analysis of 100 cells per condition, in each of 3 independent experiments.

Ribbon/compact		**Broken/extended ribbon**		**Semi-scattered**		**Full scattered**	
control vs. LIC1	≤ 0.0001	control vs. LIC1	≤ 0.0001	control vs. LIC1	0.9697	control vs. LIC1	>0.9999
control vs. LIC2	≤ 0.0001	control vs. LIC2	≤ 0.0001	control vs. LIC2	0.0735	control vs. LIC2	0.9988
control vs. LIC1+2	≤ 0.0001	control vs. LIC1+2	0.2971	control vs. LIC1+2	0.0012	control vs. LIC1+2	≤ 0.0001
LIC1 vs. LIC2	≤ 0.0001	LIC1 vs. LIC2	≤ 0.0001	LIC1 vs. LIC2	0.1790	LIC1 vs. LIC2	0.9988
LIC1 vs. LIC1+2	≤ 0.0001	LIC1 vs. LIC1+2	≤ 0.0001	LIC1 vs. LIC1+2	0.0040	LIC1 vs. LIC1+2	≤ 0.0001
LIC2 vs. LIC1+2	≤ 0.0001	LIC2 vs. LIC1+2	≤ 0.0001	LIC2 vs. LIC1+2	0.3715	LIC2 vs. LIC1+2	≤ 0.0001